

Manuscript Number: ASR-D-17-00083R2

Title: CryoSat-2 swath interferometric altimetry for mapping ice elevation and elevation change

Article Type: SI: The CryoSat Mission

Keywords: Radar altimetry; CryoSat-2; IceSat; ERS; ENVISAT; Antarctica; Greenland; Iceland; Svalbard; Sub-glacial lakes; drainage; thinning; thickening; swath processing; interferometry; Cryosphere; Ice Sheet; ice shelves; Ice Caps; glaciers; DEM; surface elevation change; climate change; sea level change; surges; surface mass balance; time-series.

Corresponding Author: Dr. Noel Gourmelen,

Corresponding Author's Institution: University of Edinburgh

First Author: Noel Gourmelen

Order of Authors: Noel Gourmelen; MariaJose Escorihuela; Andrew Shepherd; Luca Foresta; Alan Muir; Albert Garcia-Mondejar; Monica Roca; Steven G. Baker; Mark R. Drinkwater

Abstract: For more than 25 years, satellite radar altimetry has provided continuous information on the state of the cryosphere and on its contribution to global sea-level rise. The technique typically delivers maps of ice-sheet elevation and elevation change with 3 to 10 km spatial resolution and seasonal to monthly temporal resolution. Here we show how the interferometric mode of CryoSat-2 can be used to map broad (5 km-wide) swaths of surface elevation with fine (500 m) spatial resolution from each satellite pass, providing a step-change in the capability of satellite altimetry for glaciology. These swaths of elevation data contain up to two orders of magnitude more surface elevation measurements than standard altimeter products, which provide single elevation measurements based on the range to the Point-Of-Closest-Approach (POCA) in the vicinity of the sub-satellite ground track. The swath elevations allow a more dense, statistically robust time series of elevation change to be formed with temporal resolution of a factor 5 higher than for POCA. The mean differences between airborne altimeter and CryoSat-2 derived ice sheet elevations and elevation rates range from -0.931.17 m and 0.291.25 m a⁻¹, respectively, at the POCA, to -1.501.73 m and 0.041.04 m a⁻¹, respectively, across the entire swath. We demonstrate the potential of these data by creating and evaluating elevation models of: (i) the Austfonna Ice Cap (Svalbard), (ii) western Greenland, and (iii) Law Dome (East Antarctica); and maps of ice elevation change of: (iv) the Amundsen Sea sector (West Antarctica), (v) Icelandic ice caps, and (vi) above an active subglacial lake system at Thwaites Glacier (Antarctica), each at 500 m spatial posting - around 10 times finer than possible using traditional approaches based on standard altimetry products.

CryoSat-2 swath interferometric altimetry for mapping ice elevation and elevation change

N. Gourmelen^{1,2}, M.J. Escorihuela³, A. Shepherd⁴, L. Foresta¹, A. Muir⁵, A. Garcia-Mondejar³, M. Roca³, S.G. Baker⁵, M.R. Drinkwater⁶

1. School of GeoSciences, University of Edinburgh, Drummond Street, Edinburgh EH8 9XP, UK

2. IPGS UMR 7516, Université de Strasbourg, CNRS, Strasbourg 67000, France

3. isardSAT, Guildford GU2 7YG, UK

4. Centre for Polar Observation and Modelling, School of Earth and Environment, University of Leeds, Leeds LS2 9JT, UK

5. Centre for Polar Observation and Modelling, Department of Earth Sciences, University College London, Gower Street, London WC1E 6BT, UK

6. European Space Agency, ESA-ESTEC, Kelperlaan 1, 2201 AZ Noordwijk, Netherlands

1
2
3
4
5
6
7
8
9
10
11
12
13
14
15
16
17
18
19
20
21
22
23
24
25
26
27
28
29
30
31
32
33
34
35
36
37
38
39
40
41
42
43
44
45
46
47
48
49
50
51
52
53
54
55
56
57
58
59
60
61
62
63
64
65

1. Abstract

For more than 25 years, satellite radar altimetry has provided continuous information on the state of the cryosphere and on its contribution to global sea-level rise. The technique typically delivers maps of ice-sheet elevation and elevation change with 3 to 10 km spatial resolution and seasonal to monthly temporal resolution. Here we show how the interferometric mode of CryoSat-2 can be used to map broad (5 km-wide) swaths of surface elevation with fine (500 m) spatial resolution from each satellite pass, providing a step-change in the capability of satellite altimetry for glaciology. These swaths of elevation data contain up to two orders of magnitude more surface elevation measurements than standard altimeter products, which provide single elevation measurements based on the range to the Point-Of-Closest-Approach (POCA) in the vicinity of the sub-satellite ground track. The swath elevations allow a more dense, statistically robust time series of elevation change to be formed with temporal resolution of a factor 5 higher than for POCA. The mean differences between airborne altimeter and CryoSat-2 derived ice sheet elevations and elevation rates range from -0.93 ± 1.17 m and 0.29 ± 1.25 m a⁻¹, respectively, at the POCA, to -1.50 ± 1.73 m and 0.04 ± 1.04 m a⁻¹, respectively, across the entire swath. We demonstrate the potential of these data by creating and evaluating elevation models of: (i) the Austfonna Ice Cap (Svalbard), (ii) western Greenland, and (iii) Law Dome (East Antarctica); and maps of ice elevation change of: (iv) the Amundsen Sea sector (West Antarctica), (v) Icelandic ice caps, and (vi) above an active subglacial lake system at Thwaites Glacier (Antarctica), each at 500 m spatial posting – around 10 times finer than possible using traditional approaches based on standard altimetry products.

2. Introduction

1 Earth's land ice, including the Greenland and Antarctic Ice Sheets (GrIS and AIS
2 respectively), ice caps and mountain glaciers, is losing mass, and is estimated to have
3 contributed 31 mm towards global sea-level rise since 1992 (Shepherd et al. 2012,
4 Gardner et al. 2013, IPCC 2013). During this period, satellite altimetry has
5 revolutionised our ability to continuously monitor changes affecting the cryosphere,
6 providing novel and critical observations to detect, monitor, quantify and understand
7 land ice mass balance, sub-glacial water routing, ice-ocean interactions, and current and
8 potential sea-level contribution (e.g. Zwally et al. 1989, Wingham et al. 1998, Shepherd
9 et al. 2001, Shepherd et al. 2003, Zwally et al. 2005, Wingham et al. 2006a, Fricker et al.
10 2007, Pritchard et al. 2009, Wilson et al. 2010, Kaab et al. 2012, Bamber et al. 2013,
11 McMillan et al. 2014b, Gourmelen et al. 2017). Nevertheless, pulse-limited altimetry was
12 designed for ocean applications, and the relatively coarse ground resolution that can be
13 achieved with the technique has been a limiting factor for glaciology - in particular
14 when assessing changes in coastal sectors of the ice sheets and in mountain glaciers and
15 ice caps (Dehecq et al. 2013). The ground resolution of early altimeter missions was
16 limited by several factors, including the pulse- (1.6km) and beam- (10-20 km) limited
17 footprint size of radar altimeters, the relatively large separation of ground tracks (e.g.
18 20 km across track separation for IceSat at 70° of latitude) (Gourmelen et al. 2017), and
19 the inability to pinpoint the location of echoes on sloping terrain.

20 The CryoSat-2 mission, launched by ESA in 2010, achieves improved ground resolution
21 in three ways; the satellite benefits from a tight ground track network (7.5 km at the
22 equator, 1.6 km at 70° of latitude), the radar employs Synthetic Aperture Radar (SAR)
23 processing in the along-track direction to achieve a much reduced pulse-Doppler-
24 limited along-track footprint and resolution of 305m and 400 m, respectively (over a
25 flat surface); and a second receiver antenna allows the across-track location of the
26

1 ground echo to be precisely determined via radar interferometry (Drinkwater et al.
2 2005, Wingham et al. 2006). The so-called SAR Interferometry (SARIn) mode is
3
4 activated above all land ice with a significant surface slope (e.g. ice sheet margins, ice
5 caps, mountain glaciers) and provides an exact solution to the echo location uncertainty
6
7 over sloping terrains (Brenner et al. 1983). Together, these advances allow CryoSat-2 to
8
9 survey small and rugged areas of ice covered terrain, providing 5 and 6 times more data
10
11 than ICESat and Envisat, respectively (McMillan et al. 2014b). A shared characteristic of
12
13 standard radar altimetry methods is, however, that they all rely on the determination of
14
15 the Point-Of-Closest-Approach (POCA), sampling a single elevation beneath the satellite.
16
17 Here, we present a method for determining ice elevation across extended swaths of
18
19 terrain utilising the information contained within CryoSat-2 altimeter SARIn echoes.
20
21

22
23 The Interferometric mode of CryoSat-2 provides the ability to resolve substantially
24
25 more than just the elevation at the POCA. If the ground terrain slope is only a few
26
27 degrees, the CryoSat-2 altimeter operates in a manner such that the interferometric
28
29 phase of the altimeter echoes may be unwrapped to produce a wide swath of elevation
30
31 measurements across the satellite ground track beyond the POCA (Wingham et al. 2006,
32
33 Hawley et al. 2009), referred to in the remainder of this manuscript as L2swath or
34
35 simply swath (Figure 2).
36
37

38
39 An early proof of concept was performed on data acquired by the ASIRAS airborne
40
41 prototype of the CryoSat-2 instrument over the Austfonna ice cap, Svalbard, in the
42
43 spring of 2004 (Hawley et al. 2009). When evaluated against Airborne Laser Scanner
44
45 (ALS) data, swath elevations show a root mean square (RMS) departure of 1.67m in
46
47 contrast to 1.33m when only extracting the POCA. However, swath processing provided
48
49 up to 2 orders of magnitude more elevation measurements than at the POCA alone. A
50
51 study performed using CryoSat-2 data over a western section of the Devon Ice Cap
52
53
54
55
56
57
58
59
60
61
62
63
64
65

1 identified similar relative accuracy between swath and POCA (Gray et al. 2013). Recent
2 applications have shown the potential of the technique to image thinning rates at ice
3 sheet margin (Christie et al. 2016), surface depression related to supra-glacial lakes
4 (Ignéczi et al. 2016), surface elevation change related to sub-glacial lakes drainage
5 (Smith et al. 2016), ice caps mass balance (Foresta et al. 2016), and basal melting under
6 ice-shelf (Gourmelen et al. 2017) with much greater surface details.
7
8
9

10 Here, we describe a method to derive swath elevation from the SARIn mode of CryoSat-
11 2, and illustrate the benefit of the approach to derive surface elevation and time-
12 dependant surface elevation change. We present experimental elevation and elevation
13 change products derived from swath processing over several sites in the GrIS, AIS and
14 over ice caps in Iceland and Svalbard. We present validation results and compare the
15 swath measurements and derived products with existing datasets generated from
16 conventional CryoSat-2 POCA technique, as well as datasets generated from past and
17 present optical and radar airborne and spaceborne missions.
18
19
20
21
22
23
24
25
26
27
28
29
30
31
32
33
34
35
36

37 **3. Data and methods**

38 **3.1. Swath interferometric altimetry**

39
40
41
42 The swath algorithm consists of (i) identifying suitable waveform echoes within the L1b
43 SARIn mode product based on high phase coherence, amplitude and surface slopes, the
44 threshold to use will depend on the local conditions (Gray et al. 2013, Foresta et al.
45 2016, Gray et al. 2016); (ii) determining the correct phase ambiguity (unwrapping) (as
46 wrapping of the phase occurs for an arrival angle greater than $\sim 0.54^\circ$) by a combination
47 of spatial unwrapping and quality control using a reference digital elevation model
48 (Gray et al. 2015, Foresta et al. 2016) and (iii) mapping the range, across-track look
49
50
51
52
53
54
55
56
57
58
59
60
61
62
63
64
65

1 angle, platform attitude and orbit parameters of each echo into a swath comprised of
2 multiple elevation points above a reference ellipsoid (Figure 3) (Wingham et al. 2006,
3
4
5 Hawley et al. 2009, Gray et al. 2013, Foresta et al. 2016).
6

7 **3.1.1. Input data**

8
9
10 Swath processing takes as input multi-looked echo (L1b product, baseline C) from the
11 Synthetic Aperture Radar Interferometric (SARIn) mode of CryoSat-2, containing the
12
13 power, interferometer phase and coherence waveforms. All necessary input data are
14
15 contained in the L1b product delivered by ESA (<ftp://science-pds.cryosat.esa.int>) with
16
17 the exception of an external reference digital elevation model (DEM_{ref}).
18
19
20
21
22

23 **3.1.2. Smoothing**

24
25
26 To reduce instrument noise, the phase and amplitude are filtered by recreating the
27
28 interferogram, filtering its real and imaginary components with a low pass filter and
29
30 retrieving the phase from the smoothed interferogram (Gray et al. 2013). We filter each
31
32 waveform independently with a filter size equal to 3 bins to limit the loss of spatial
33
34 resolution.
35
36
37
38
39

40 **3.1.3. Local phase unwrapping**

41
42
43 Phase difference can only be known within a $[-\pi \pi]$ interval and so a phase ambiguity
44
45 will be present when the angle of arrival exceeds about half a degree, a situation that
46
47 can occur when e.g. the ground-surface slope exceeds about half a degree. Correction of
48
49 phase ambiguities requires a phase unwrapping procedure which is applied to each
50
51 waveform separately by adding or subtracting 2π when the absolute phase change
52
53 between 2 consecutive bins exceeds π . In order to minimize phase unwrapping errors,
54
55
56
57
58 phase values for which the coherence is below a threshold of 0.8 is masked.
59
60
61
62
63
64
65

3.1.4. Generation of Latitude, longitude and elevation

The look angle θ is such that

$$\theta = \arcsin\left(-\frac{\lambda}{2\pi} \frac{\delta\varphi}{B}\right) - \beta \quad (1)$$

with λ the wavelength, $\delta\varphi$ the phase difference, B the interferometer baseline and β the roll angle. The range R at each waveform sample n as:

$$R(n) = \frac{c}{2} \cdot \left(T + \frac{1}{2 \cdot F_r} \left(n - \frac{N}{2} \right) \right) \quad (2)$$

where N is the total number of waveform samples, n is the sample number in the $[0, N-1]$ interval, T is the window delay, in seconds, at bin $\frac{N}{2}$, F_r is the instrument sampling frequency, and c is the speed of light.

3.1.5. Global phase unwrapping

We introduce an additional step to account for phase ambiguities; the independent DEM_{ref} is used to guide the phase unwrapping steps where phase ambiguity cannot be resolved from simple unwrapping (e.g. when the entire waveform is affected by a phase ambiguity). This approach potentially improves the measure of elevation for echoes whose across-track angle is above $\sim 0.54^\circ$ for all or part of the beam limited footprint, a condition found frequently for ice caps and locally along ice sheet margins.

In the presence of slopes exceeding $\sim 0.54^\circ$, the conventional unwrapping procedure described above will not be able to resolve the phase ambiguity as the first arrival measurement will be affected by a phase shift; in this situation we will need to apply a 'global' phase correction, i.e. adding or subtracting a suitable multiple of 2π to the phase values of a waveform. Without accounting for this correction, elevation estimates can be off by tens of meters and their location off by a few kilometers.

1 We implemented a procedure involving a reference DEM. For each waveform, latitude,
2 longitude and elevation are computed for a number of 2π multiples (positive and
3 negative). The correct 2π ambiguity is then chosen using two metrics. Firstly, we find
4 the phase ambiguity that minimizes the elevation difference between CryoSat-2 swath
5 and the DEM_{ref} :
6
7
8
9
10

$$\sum_{i=1}^N |h_i - DEM_{ref_i}| \quad (3)$$

11 with h_i and DEM_{ref_i} respectively the swath elevation and DEM_{ref} at the waveform
12 sample number i . The second metric is the dispersion of the elevation difference defined
13 as the Median Absolute Deviation:
14
15
16
17
18
19
20
21
22

$$MAD_{hd} = median|hd - median(hd)| \quad (4)$$

23 where hd is a vector of the difference between the swath elevations at each waveform
24 samples and the corresponding reference elevation. This second metric stems from the
25 fact that an erroneous phase ambiguity will impact on the slope of the surface
26 topography, hence leading to a large value of MAD_{hd} (Figure 4). This second metric adds
27 robustness to the determination of the phase ambiguity.
28
29
30
31
32
33
34
35
36
37

38 Given the magnitude of the impact of a phase ambiguity on the planimetric positioning,
39 elevation and surface slope of the swath measurement (Figure 4), and although the
40 reference DEM need to be relatively accurate or recent, a certain level of difference is
41 acceptable. However, due to the complexity of surface terrain it is difficult to predict the
42 level of accuracy needed. Distinct reference DEMs are used in this study for GrIS
43 (Howat, Negrete & Smith 2014), AIS (Fretwell et al. 2013), Iceland (Landmælingar
44 Íslands, www.lmi.is), and Svalbard (McMillan et al. 2014a).
45
46
47
48
49
50
51
52
53
54
55

56 We note that phase ambiguity is not only affecting swath but also POCA processing were
57 a reference DEM is also needed to resolve phase ambiguity (Gray et al. 2015).
58
59
60
61
62
63
64
65

3.2. Digital elevation model and rates of surface elevation change

Because of the increased data density, L2swath altimetry provides a capability to determine changes in ice elevation at the maximum spatial resolution of the CryoSat-2 instrument, up to 0.4 km in the platform's along-track direction. To assess this capability, we computed ice sheet surface elevation changes within 500 m grid cells by fitting a plane to the raw L2swath elevation measurements within a grid cell using a model function of spatial and temporal elevation change of the form:

$$Z(x, y, t) = ax + by + c + dt \quad (5)$$

where Z is the swath elevation, x and y are the easting and northing coordinates of each swath data point, respectively, and t is the time of data acquisition (Foresta et al. 2016).

Surface elevation and elevation change are then determined from the model parameters a , b , c and d ; a corresponding to the eastward linear elevation trend, b to the northward linear elevation trend, c a constant, and d the linear rate of temporal elevation change.

In this model the spatial variation in elevation is determined as a bilinear function and the temporal variation of elevation as a linear term. The power field, P , is used to weight the individual elevation measurements during the inversion process; for each grid cell, the weight, w , is defined as:

$$w = \frac{P^2}{\max(P)^2} \quad (6)$$

This weighting strongly penalises measurement with low power. This inversion approach is similar to solutions applied to CryoSat-2 POCA data (McMillan et al. 2014b), only with a simplification of the terrain slope terms made possible by the finer spatial distribution of the input data. The use of either linear or quadratic polynomial to model

1 the terrain slope within a grid cell does not affect markedly the values of elevation
2 change compared to airborne data, with less than 1% difference under each scenario.
3

4 The advantage of this approach to determine a gridded CryoSat-2 swath digital
5 elevation model (CSDEM), with respect to other approaches that average measurements
6 acquired over a long time-period, is the ability of our model to account for the time-
7 dependant aspect of the topography in regions of rapid and complex changes, and
8 therefore to generate a DEM of high-temporal fidelity.
9
10
11
12
13
14
15

16 **3.3. Validation**

17 Swath elevation and derived gridded products are validated using surface elevation and
18 elevation change from the NASA Operation IceBridge (OIB) Airborne Topographic
19 Mapper (ATM) campaigns (Krabill 2016, Krabill 2015). OIB campaigns are a series of
20 airborne missions to map Arctic and Antarctic ice sheets with laser altimetry between
21 2009 and 2016 (filling the gap between ICESat and ICESat-2). We have used the OIB
22 ATM L2 Icessn Elevation, Slope, and Roughness product, Version 1. The ATM data are
23 referenced to the ITRF-2005 reference frame and projected onto the WGS-84 ellipsoid.
24
25 The footprint size of each individual elevation measurement is 1 m, which is set by the
26 laser beam divergence (Krabill 2016). Absolute elevation accuracy from the ATM is
27 usually about 10 cm or better (Krabill 2016) with geolocation accuracies of better than
28 1 m (Schenk, Csatho & Lee 1999). Specifically for the OIB campaigns, the parameters of
29 the ATM system are estimated to be (i) 74 cm horizontal accuracy, (ii) 6.6 cm vertical
30 accuracy, and (iii) 3 cm vertical precision (Martin et al. 2012).
31
32
33
34
35
36
37
38
39
40
41
42
43
44
45
46
47
48
49
50
51

52 Due to the rapid changes at the margins of the ice sheets, only elevation data acquired
53 as close in time as possible has been considered for validation purposes. The validation
54 activities have also avoided rapid melting and precipitation periods and have been
55
56
57
58
59
60
61
62
63
64
65

1 therefore concentrated for the northern hemisphere in the months of March, April and
2 May and for the Southern Hemisphere in the months of October and November covered
3 by OIB ATM acquisitions.
4

5 For each CryoSat-s measurement we select the nearest validation measurement that
6 satisfies the spatial and temporal baseline thresholds of 50m and 10 days respectively.
7

8 For the gridded CSDEM and rates of elevation change products, the spatial criterion is
9 that the validation measurement is within half the grid spacing, or 250m, and the
10 temporal criterion is 1 repeat cycle (369 days) from the time stamps of the CSDEM
11 which are usually set at the first CryoSat-2 record, i.e. 07/2010. We then define a
12 measurement bias as the median value of the difference between the L2swath and the
13 validation elevation, and a measurement dispersion as the Median Absolute Deviation
14 defined as:
15

$$16 \text{MAD} = \text{median}(|(Z_n - Z_n^{val}) - \text{median}(Z_n - Z_n^{val})|) \quad (7)$$

17 where Z_n are the swath elevations and Z_n^{val} are the corresponding validation records.
18

19 Our validation test sites are located at the margins of the two ice sheets and include the
20 glaciers of Petermann and Jakobshavn glaciers (GrIS), and the Pine Island and Thwaites
21 glaciers in the Amundsen Sea sector of AIS.
22

23 **4. Results**

24 **4.1. Swath elevation**

25 **4.1.1. Data coverage and volume**

26 A capacity to sample elevation at locations beyond the POCA means that L2swath
27 provides a snapshot of terrain in both along-track and across-track directions, turning
28 CryoSat-2 into an instantaneous two-dimensional mapping sensor. The across-track
29 width of swaths can reach several kilometres, the exact extent depending on surface
30
31
32
33
34
35
36
37
38
39
40
41
42
43
44
45
46
47
48
49
50
51
52
53
54
55
56
57
58
59
60
61
62
63
64
65

1 slope (Figure 5). Considering a range of glaciological targets, L2swath processing
2 typically retrieves between 10 and 100 distinct elevation measurements from a single
3 altimeter echo, by contrast to a single elevation measurement in the standard L2
4 product. The improvement in data quantity for each of the validation sites is provided in
5 Table 1.
6
7
8
9
10
11

12 **4.1.2. Validation**

13
14 We evaluated the accuracy of L2swath data over GrIS and AIS marginal regions with
15 respect to 344×10^3 independent airborne altimeter elevation measurements acquired
16 between 2011 and 2014 (Figure 8 & Table 1). The differences between the airborne and
17 CryoSat-2 swath elevations is -1.50 ± 1.73 m; the -1.5 m bias reflects the greater
18 penetration of Ku-band radar into the snow and firn compared to the ATM. For
19 comparison, the differences between the airborne and POCA observations is $-0.93 \pm$
20
21
22
23
24
25
26
27
28
29
30
31
32
33
34
35
36
37
38
39
40
41
42
43
44
45
46
47
48
49
50
51
52
53
54
55
56
57
58
59
60
61
62
63
64
65

66 **4.1.3. Baseline C versus baseline B**

67 In 2015, CryoSat-2's Instrument Processing Facilities was updated to Baseline C,
68 improving the product's quality and correcting several biases (Scagliola, Fornari 2015).
69 One improvement included in Baseline C is the removal of the waveform cut initially
70 introduced in Baseline B during the oversampling of the 20 Hz waveform, that led to a
71 loss of information. Baseline C now provides a range window of 240 m, double in length
72 to that of baseline B. This leads to an increase in the number of elevations that L2swath
73 is able to deliver (Figure 6).
74
75
76
77
78
79
80
81
82
83
84
85
86
87
88
89
90
91
92
93
94
95
96
97
98
99
100

101 **4.1.4. Roll bias**

102 An inaccurate value of satellite's roll angle will impact on the positioning of the
103 elevation measurements, with a greater impact with large off-nadir angle. A roll bias of

1 0.1062° was identified in CryoSat’s baselineB dataset and corrected in CryoSat new
2 latest release, baseline C (Scagliola, Fornari 2015). It has been suggested that a residual
3 roll bias is present in CryoSat’s baseline C (Gray et al. 2016). To explore this possibility,
4 we calculate swath elevations using look angles calculated by introducing arbitrary roll
5 angle biases β_b as follows:
6
7
8
9
10

$$\theta = \arcsin\left(-\frac{\lambda}{2\pi} \frac{\delta\varphi}{B}\right) - (\beta + \beta_b) \quad (8)$$

11 We then use OIB elevation to explore the roll angle bias impact on the L2swath-OIB
12 elevation differences (Figure 7). When a roll angle bias is present, ascending and
13 descending orbit will be affected in opposite direction leading to a double-peak
14 histogram of the L2swath-OIB elevation differences (Figure 7, lower-left). For a correct
15 value of roll angle, the histogram will have the expected single peak (Figure 7, lower-
16 left). We then solve for the roll bias that minimises the histogram dispersion and found
17 a value of 0.007° m. If uncorrected, this directly translates in an offset of 87 m in
18 geolocation in the across track direction, and in a vertical offset of 0.01 m at nadir and of
19 1.60 m at the edge of the footprint, of the elevation retrieval.
20
21
22
23
24
25
26
27
28
29
30
31
32
33
34
35
36
37

38 This value is likely to vary however as the roll bias depends on the temperature of the
39 platform. There are two causes of temperature changes: short term variations (the
40 platform is facing the sun with different incidents angles within an orbit) and long term
41 variation (the orbit plane of the platform has different incidents angles within the 369
42 day cycle).
43
44
45
46
47
48
49

50 The noise of the roll is higher when the measurements are given by the Star Tracker
51 that is not the coldest, but also there is a long-term variation due to the bending of the
52 bench where the Star Tracker are placed.
53
54
55
56
57
58
59
60
61
62
63
64
65

1 The new CryoSat-2 baseline-C incorporates a Star Tracker processor in charge of
2 computing the attitude measurements provided on the products with the stated roll
3 bias and some smoothing algorithms. With that smoothing the noise of the roll
4 measurement is compensated but the long-term variation cannot be addressed at it
5 would require a long term analysis. The external calibration analysis using data over a
6 Transponder indicates that the roll bias in Baseline C is $0.0069 \pm 0.003^\circ$ (A.Garcia-
7 Mondejar et al., 2017).
8
9

10 A dataset of re-calibrated attitude information recently released by ESA
11 (<https://earth.esa.int/web/guest/missions/esa-eo-missions/cryosat/str-attref>) is also
12 tested (Figure 7) and show that it largely corrects for the roll angle bias observed in the
13 current baseline C dataset. The updated attitude will be incorporated in an upcoming
14 baseline D release by ESA.
15
16

17 This exercise also demonstrates that swath processing could be a complementary
18 approach to transponders for calibrating the attitude of interferometric radar
19 altimeters with vastly improved spatial and temporal coverage.
20
21
22
23
24
25
26
27
28
29

30 **4.2. Gridded Digital elevation model and rates of surface elevation change**

31 We generated and validated gridded DEMs and rates of surface elevation change at 500
32 m grid spacing for the Jakobshavn area (west GrIS) and for the Amundsen Sea sector of
33 West Antarctica. In total we retrieve an elevation for 98.8% (Jakobshavn area) and
34 98.2% (Amundsen Sea sector) of the area over the grounded ice sheets. For comparison,
35 studies at the scale of the entire AIS using CryoSat-2 POCA data found 96% coverage at
36 5 km by 5km, and from Envisat cross-over POCA found 32% coverage at 10 km by 10km
37 (Shepherd et al. 2012, McMillan et al. 2014b). We also show case examples over the
38 Law Dome (East Antarctica) as well as over ice caps in Iceland.
39
40
41
42
43
44
45
46
47
48
49
50
51
52
53
54
55
56
57
58
59
60
61
62
63
64
65

4.2.1. Digital elevation model

Validation of the L2swath DEM at 500 m grid spacing indicates a bias of -1.4 m and a dispersion of 1.8 m when swath elevation are compared to 39,139 collocated airborne measurements from OIB over the Jakobshavn area (Figure 8). A similar intercomparison over the Amundsen Sea sector indicates bias of -1.7 m and a dispersion of 2.0 m when compared to 29,362 airborne measurements over grounded ice (Table 1) and -1.5 m and a dispersion of 1.2 m over floating ice (Gourmelen et al. 2017). Improved spatial resolution offered by the greater density of swath measurements allows far greater definition of glacial terrain than has been possible to date. For example, at Law Dome in East Antarctica, a CSDEM produced at 500 m grid spacing (Figure 9) clearly identifies surface features on length scales of 500 to 4000 m which are common in airborne data sets, but are not resolved in continental-scale products (Fretwell et al. 2013). Over the east flank of law Dome, a system of surface gashes is well defined at 500 m resolution; the gashes' system is the surface expression of a large canyon system in the underlying bedrock (Figure 9).

4.2.2. Surface elevation change

4.2.2.1. Multi-annual change

In the Amundsen Sea Sector of West Antarctica, rates of elevation change determined from L2swath show a remarkable level of detail when compared to results that can be achieved using POCA elevation data alone (Figure 10 & Figure 11). Although CryoSat-2 POCA data are recorded within a much smaller ground footprint than conventional pulse-limited altimetry, they lead to only a modest (factor 2) improvement in spatial resolution of elevation changes due to the relatively long orbit repeat cycle which requires measurements to be collated in space. In contrast, L2swath data allow for a 10-

1 fold improvement in spatial resolution of elevation changes (Table 1). Measurements
2 with such fine sampling allow the detailed pattern of thinning along tributaries of the
3 Pine Island, Thwaites, Smith, Kohler and Pope Glaciers to be clearly identified, and
4 ensure that signals of elevation change can be retrieved up to the ice sheet margin even
5 over the floating ice shelves (Gourmelen et al. 2017). Over smaller features such as ice
6 caps the benefit of L2swath is also apparent with a dramatic increase in surface
7 coverage (Figure 11). When comparing L2swath-derived rates of elevation change with
8 POCA-derived estimates and with estimates of elevation change determined from
9 repeat airborne surveys over the same period (Krabill 2015), the L2swath data are in
10 excellent agreement. For the Amundsen Sea Sector (Figure 10), we observe a mean
11 difference between swath and OIB of $0.04 \pm 0.92 \text{ m a}^{-1}$, this value is comparable to the
12 estimated certainty ($0.40 \pm 0.95 \text{ m a}^{-1}$) of POCA-derived elevation changes in the same
13 region (McMillan et al. 2014b). Over ice caps we also observe a very good agreement
14 and no noticeable impact of surface slopes (Figure 12) (Foresta et al. 2016).

34 **4.2.2.2. Seasonal or transient change**

35 CryoSat's repeat cycle of 369 days limits the temporal resolution at which localised
36 changes can be mapped. Generating swath of elevation instead of POCA leads to overlap
37 between adjacent tracks, leading to an increase in the temporal resolution at which
38 elevation change can be determined. The improvement in spatial resolution is greater
39 for deformation that are spatially and temporally localised. With L2swath data, we
40 observe a 35-fold increase in the probability of sampling an area of 500 m^2 in size at 1-
41 90 day time step (length of CryoSat-2's orbital sub-cycle) (Figure 13).

42 For example, the L2swath observations clearly identify a cluster of dislocated sites in
43 the interior of the Thwaites Glacier drainage basin (Figure 14) (Smith et al. 2016). In

1 this 860 km² region, four sites of between 100 and 360 km² have lowered by 6 to 13 m
2 over a 1 year period, similar to patterns of surface lowering above subglacial lakes that
3 have drained in other sectors of Antarctica (Fricker et al. 2007, Wingham et al. 2006b).
4
5 Observations using POCA data only partially cover the area (Figure 14) leading to an
6
7 incomplete mapping of the subsidence features and a 30% error in the total subsidence
8
9 volume.
10
11

12
13
14 A second example of highly-localised and rapid changes in ice elevation mapped by
15 forming and differencing sequential CryoSat-2 L2swath measurements is shown in
16
17 Figure 15. In the summer of 2014, the north-west sector of the Vatnajökull ice cap in the
18
19 region of the Bárðarbunga caldera, Iceland, experienced high seismic activity followed
20
21 by a volcanic eruption off-ice north of the seismic swarm (Sigmundsson et al. 2015). The
22
23 entire caldera deformation was imaged by 6 swaths of CryoSat-2 data acquired just
24
25 before and after the event, revealing the extent of the subsidence that affected the
26
27 region of the ice cap in the months following the seismic activity (Figure 15). The
28
29 L2swath data reveal that a 25 km² region subsided by over 40 m in the 4 months that
30
31 followed the onset of seismic activity, amounting to a 0.75 km³ deflation which has been
32
33 confirmed by Airborne LIDAR and GPS surveys (Reykjavik Institute of Earth Sciences).
34
35 The width of the swath was sufficient to map the entire subsidence event, when POCA
36
37 elevation data would only have provided a coarse picture.
38
39

40
41
42 Seasonal patterns of elevation change, e.g. related to the seasonal cycle of accumulation
43
44 and ablation, have been retrieved from altimetry over large region, at the scale of an
45
46 entire ice sheet (McMillan et al. 2016) or ice cap (Gray et al. 2015). Increase spatial
47
48 resolution means that we can start focussing seasonal analysis from radar altimetry
49
50 over smaller targets. An example over the Vatnajökull ice cap (Iceland) shows the
51
52 seasonal pattern in elevation related to accumulation and ablation partitioned between
53
54
55
56
57
58
59
60
61
62
63
64
65

1 the accumulation (above 1200 m) and ablation area (below 1200m) (Figure 16)
2 (Foresta et al. 2016).
3

4 **5. Discussion**

5
6
7
8 The separation of CryoSat-2's ground track ranges from 7.5 km at the equator to less
9 than 1.6 km at latitudes higher than 70°. However, the actual separation of elevation
10 measurements recorded by the altimeter can be significantly larger than this, because
11 the POCA is dependent upon the surface slope and tends to follow topographic ridges.
12 This effect occurs in marginal sectors of the polar ice sheets and ice caps and across
13 mountain glaciers, where the terrain is typically steep. In such instances, features that
14 are kilometre-scale or smaller may be under-sampled or missed altogether by standard
15 altimeter measurements recorded at the POCA alone. L2swath data, however, overcome
16 this problem because they map broad and continuous swaths of ice covered terrain,
17 allowing surface elevation and surface elevation changes to be determined with 10
18 times finer spatial resolution than conventional altimetry (Figure 9).
19
20
21
22
23
24
25
26
27
28
29
30
31
32
33

34 In addition to providing a denser network of elevation measurements around the POCA,
35 swath interferometry allows for the retrieval of elevation data where the conventional
36 POCA altimetry approach fails. This situation occurs where the POCA falls on incoherent
37 surfaces, leading to retracker failure, or in regions of complex ice topography where the
38 POCA tends to concentrate along topographic highs leaving topographic lows uncharted
39 (McMillan et al. 2013). In contrast, L2swath is able to image the ice terrain beyond the
40 POCA and to measure elevation in surface depressions providing they are within the
41 limits of the altimeter's sampling window (corresponding to 240 m elevation range for
42 CryoSat-2 baseline C).
43
44
45
46
47
48
49
50
51
52
53
54
55
56
57
58
59
60
61
62
63
64
65

1 The step-change in the yield of valid elevation measurements means that L2swath
2 provides an opportunity to extract continuous surface elevation at enhanced spatial
3 resolution in comparison to previous altimetry-based products (Fretwell et al. 2013,
4 DiMarzio et al. 2007a, Bamber, Gomez-Dans & Griggs 2009). Although digital elevation
5 models (DEMs) are often distributed on fine (500 to 1000 m) spatial grids, actual
6 observations are generally oversampled. The effective resolution of existing products is
7 typically an order of magnitude lower (DiMarzio et al. 2007a, DiMarzio et al. 2007b,
8 Griggs, Bamber 2009), and many grid points are not constrained by measurements at all
9 due to the paucity of primary observations. In addition to improved coverage, the
10 accuracy of DEM's derived from swath altimetry is also well within that of existing
11 products. The example elevation models we have produced demonstrate that
12 continuous DEM's exhibiting true sub-kilometre spatial resolution are feasible with
13 swath interferometric altimetry. The technique is now approaching the capabilities of
14 airborne surveys (Howat, Negrete & Smith 2014, Krabill 2016), and while the spatial
15 resolution of the gridded products obtained here is not commensurate with that
16 achieved by high-resolution sensors (Berthier et al. 2014, Howat et al. 2015, A. Dehecq
17 et al. 2016), the technique benefits from frequent and regular, day-night, all-weather
18 and global coverage as well as seamless aggregation. We also note that the non-gridded
19 swath product can resolve elevation at meter-scale spatial resolution (Gray et al. 2016)
20 in par with high-resolution imaging sensors. As a consequence of the increased spatial
21 sampling, L2swath data allow ice elevations to be mapped with higher temporal
22 frequency. Although the CryoSat-2 orbit repeat cycle is 369 days, which limits the
23 observation of rapidly changing processes, the width of L2swath swaths provides
24 greater overlap between adjacent ground tracks. At 70° latitude this translate into a
25 three, five, ten and 35-fold increase in temporal sampling respectively at 5, 3, 1 and 0.5
26
27
28
29
30
31
32
33
34
35
36
37
38
39
40
41
42
43
44
45
46
47
48
49
50
51
52
53
54
55
56
57
58
59
60
61
62
63
64
65

1 km posting when compared to POCA measurements alone (Figure 13). Improved
2 sampling of ice elevation changes will improve our understanding of key glaciological
3 processes. Although half of today's sea level change is due to ice mass losses (IPCC
4 2013), these losses are predominantly occurring in mountainous and coastal regions
5 which present a challenge to conventional altimetry. However, because L2swath
6 performs well over rugged ice covered terrain, more accurate estimates of glacier and
7 ice sheet mass balance will become possible. The movement of water between lakes at
8 the base of the Antarctic (Fricker et al. 2007, Wingham et al. 2006b) and Greenland
9 (Joughin et al. 1996) ice sheets, has the capacity to affect ice flow (Smith et al. 2016,
10 Stearns, Smith & Hamilton 2008), release freshwater into the ocean (Fricker et al.
11 2007), deform glacial landforms (Lewis et al. 2006), and disturb subglacial habitats
12 (Siegert et al. 2005). Although the surface expression of sub-glacial lake drainage has
13 been recorded in pulse-limited (Wingham et al. 2006b) and laser (Fricker et al. 2007)
14 altimetry, conventional measurements acquired at the POCA have been shown to
15 preferentially sample the highest sections of surface depressions (McMillan et al. 2013).
16 A consequence is that POCA tends to underestimate the deflation. For example,
17 estimates of the volume change within depressions above presumed sub-glacial lake
18 sites in the Thwaites Glacier catchment (Figure 14) based on POCA L2swath elevation
19 data differ by more than 40%. L2swath resolves this problem, and will lead to an
20 improved inventory of active sub-glacial lakes (Smith et al. 2009, Wright, Siegert 2012)
21 and their water mass budgets. In Greenland and on the Antarctic Peninsula, supra-
22 glacial lakes similarly create and occupy depressions on the ice sheet surface (Liestl,
23 Repp & Wold 1980, Scambos et al. 2000, McMillan et al. 2007), and the ability to map
24 their shape in full (Ignéczi et al. 2016) will lead to an improved characterisation of their
25
26
27
28
29
30
31
32
33
34
35
36
37
38
39
40
41
42
43
44
45
46
47
48
49
50
51
52
53
54
55
56
57
58
59
60
61
62
63
64
65

1 seasonal hydrology which is believed to influence rates of ice flow (Das et al. 2008) and
2 ice shelf stability (Phillips, Rajaram & Steffen 2010).
3

4 **6. Conclusions**

5
6
7
8 Trends in the elevation of ice sheets, ice caps, and mountain glaciers derived from
9 satellite altimetry are a key observation for quantifying and understanding the impacts
10 of environmental change. We have described how swath interferometric processing of
11 CryoSat-2 data provides a step change in the quantity of valid elevation data that can be
12 derived from satellite radar altimetry. By applying the technique to CryoSat-2
13 measurements acquired over a range of geophysical targets, we demonstrate that a
14 tenfold gain in the density of data can be achieved in comparison to conventional
15 satellite altimetry performed only at the POCA. Furthermore, we show that the increase
16 in data density is not detrimental to data quality, with only a modest (up to 50% and
17 surface dependant) degradation in the bias and variability of elevation measurements
18 relative to standard POCA approaches. L2swath also provide a near continuous
19 elevation field, making it possible to form digital elevation models and to map rates of
20 surface elevation change at a true resolution of 500 m - an order of magnitude finer than
21 is the current state of the art for the continental ice sheets. This leads to a more accurate
22 picture of the complexity of surface topography and patterns of surface elevation
23 change within ice stream tributaries, along the ice sheet margins, ice shelves, and in
24 surface depressions linked with ice sheet hydrology. Applied extensively, these new
25 observations will transform our understanding of cryospheric change.
26
27
28
29
30
31
32
33
34
35
36
37
38
39
40
41
42
43
44
45
46
47
48
49
50
51

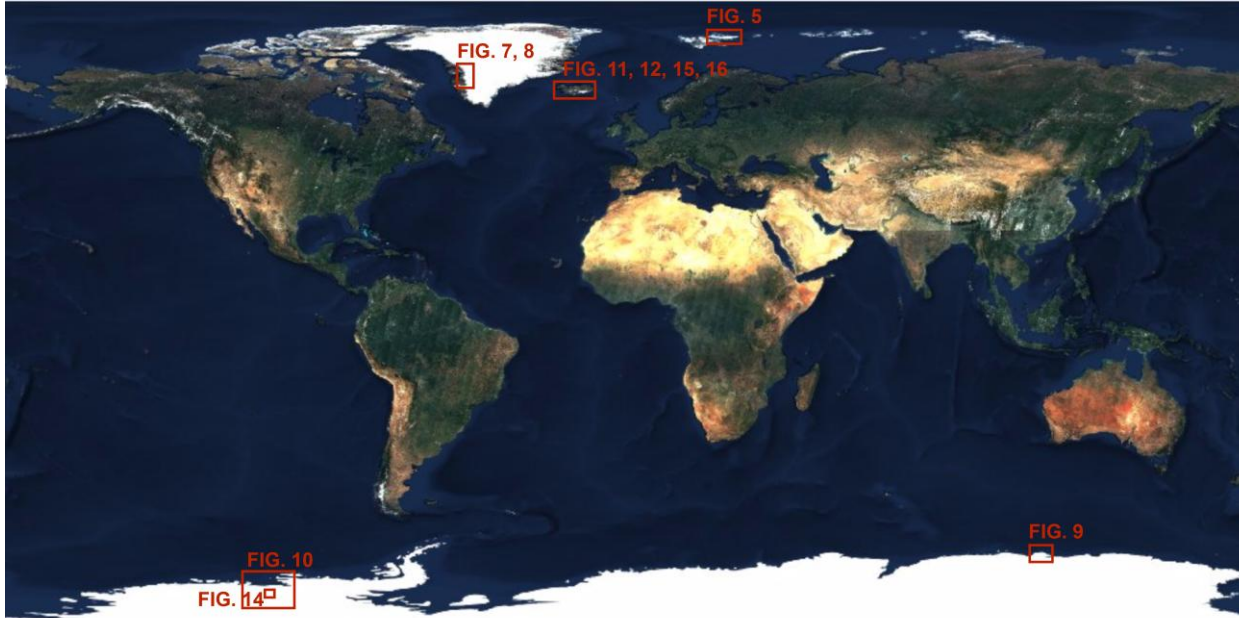
52 **8. Acknowledgments**

53 This work was supported by European Space Agency contracts CryoTop
54
55
56
57
58 4000107394/12/I-NB and CryoTop evolution 4000116874/16/I-NB (NG). The CryoSat-
59
60
61
62
63
64
65

2 satellite altimetry data are freely available from the European Space Agency
(<https://earth.esa.int/web/guest/data-access>). The IceBridge airborne altimetry data
are freely available from the National Snow and Ice Data Centre
(<https://nsidc.org/data/icebridge/>). We are grateful to two anonymous reviewers and
the editor, whose comments have significantly improved the manuscript

1
2
3
4
5
6
7
8
9
10
11
12
13
14
15
16
17
18
19
20
21
22
23
24
25
26
27
28
29
30
31
32
33
34
35
36
37
38
39
40
41
42
43
44
45
46
47
48
49
50
51
52
53
54
55
56
57
58
59
60
61
62
63
64
65

1
2
3
4
5 **9. Figures and Tables**
6
7



29
30 Figure 1: Map with figures location. Background is Sentinel-2 cloudless. Contains
31
32 modified Copernicus Sentinel data 2016, EOX.
33
34
35
36
37
38
39
40
41
42
43
44
45
46
47
48
49
50
51
52
53
54
55
56
57
58
59
60
61
62
63
64
65

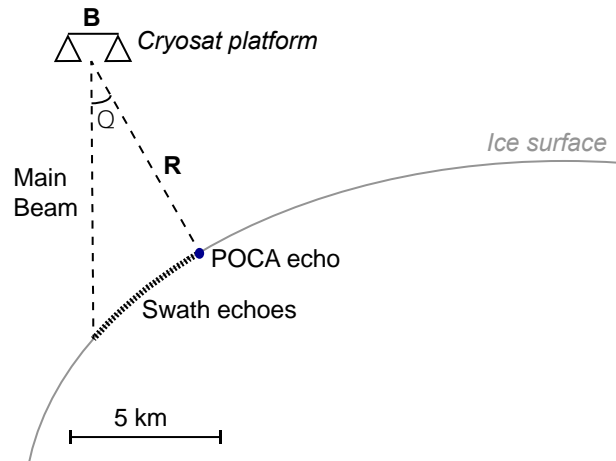


Figure 2: Swath interferometry retrieves elevation across the satellite ground track beyond the POCA. B is the interferometric baseline, R is the slant range, θ is the look angle.

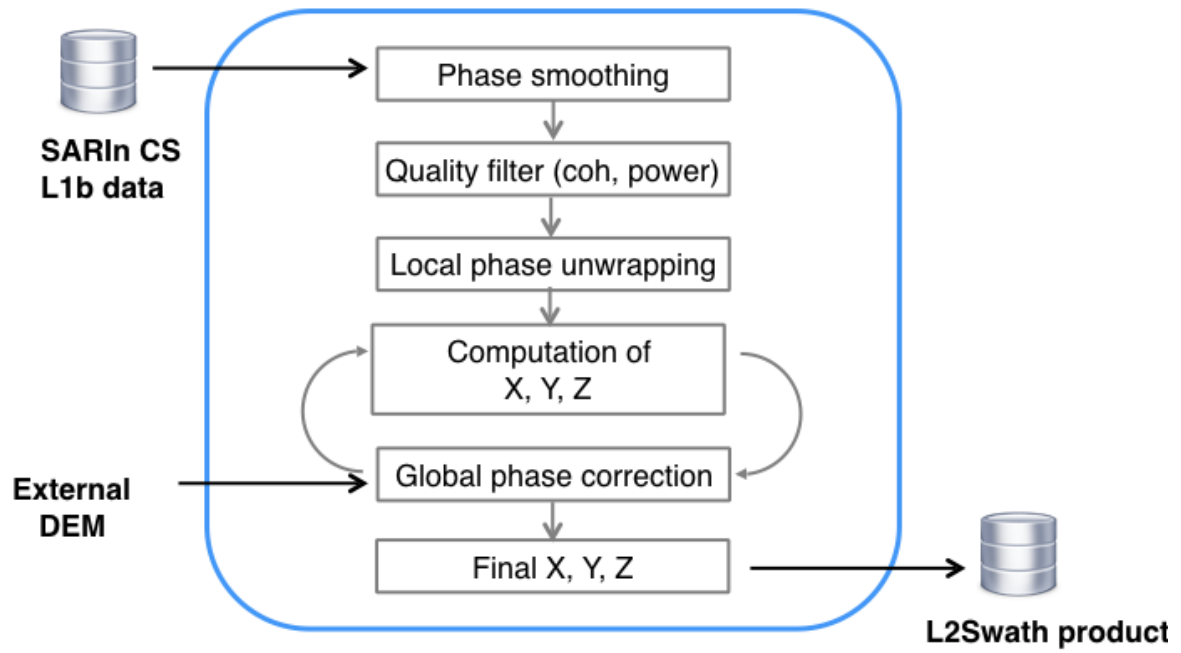


Figure 3: Swath processing workflow.

1
2
3
4
5
6
7
8
9
10
11
12
13
14
15
16
17
18
19
20
21
22
23
24
25
26
27
28
29
30
31
32
33
34
35
36
37
38
39
40
41
42
43
44
45
46
47
48
49
50
51
52
53
54
55
56
57
58
59
60
61
62
63
64
65

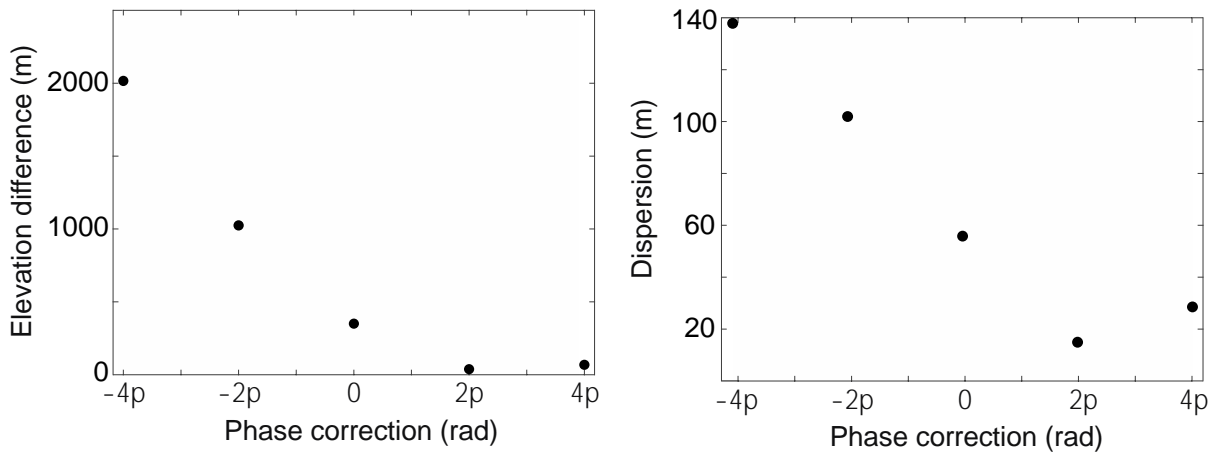
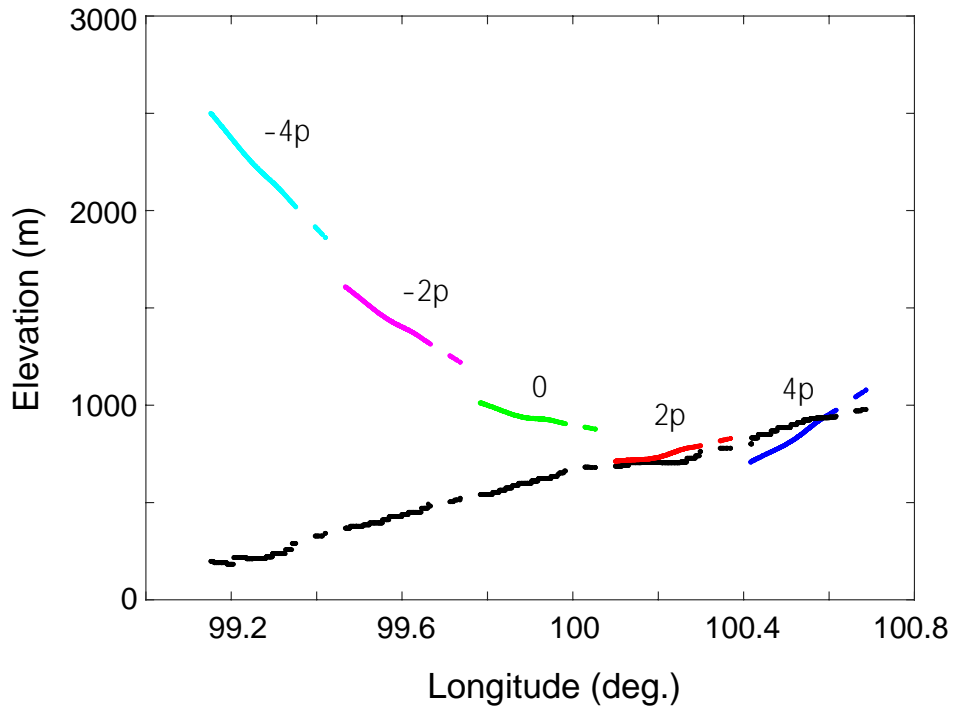


Figure 4: (top) Surface elevation of swath-processed CryoSat data to which 5 distinct values of phase ambiguity $([-4 -2 0 2 4] \cdot \pi)$ have been applied and corresponding topography of the reference elevation dataset (black dots). Elevation difference (bottom left) and dispersion (bottom right) between swath-derived elevation and reference DEM_{ref} for various phase ambiguity. The correct phase ambiguity in this example is $+2\pi$.

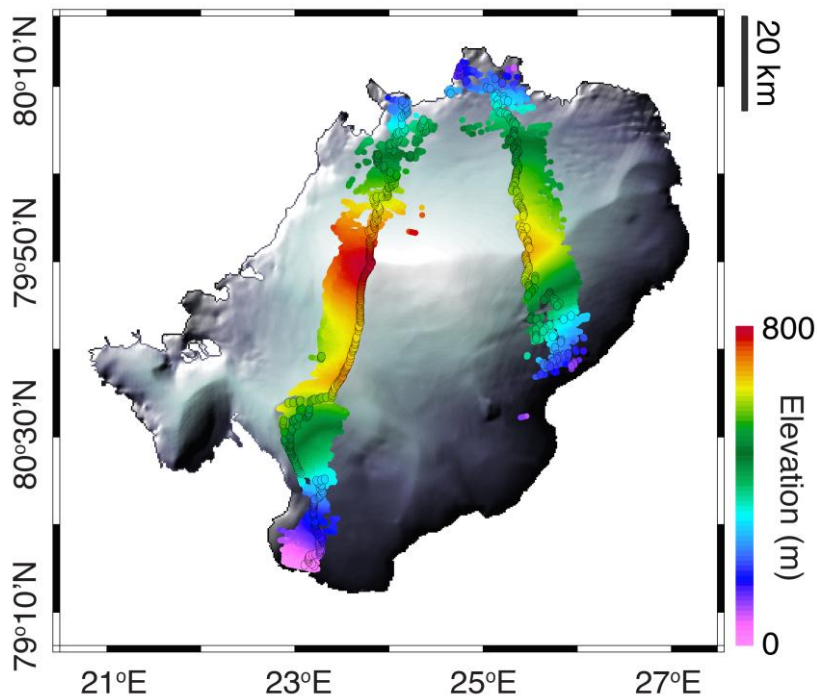


Figure 5: Austfonna ice cap, Svalbard, surface elevation determined using two orbits of swath (colour) and POCA (open circles) CryoSat-2 altimetry; swath altimetry delivers a 75-fold increase in spatial sampling.

1
2
3
4
5
6
7
8
9
10
11
12
13
14
15
16
17
18
19
20
21
22
23
24
25
26
27
28
29
30
31
32
33
34
35
36
37
38
39
40
41
42
43
44
45
46
47
48
49
50
51
52
53
54
55
56
57
58
59
60
61
62
63
64
65

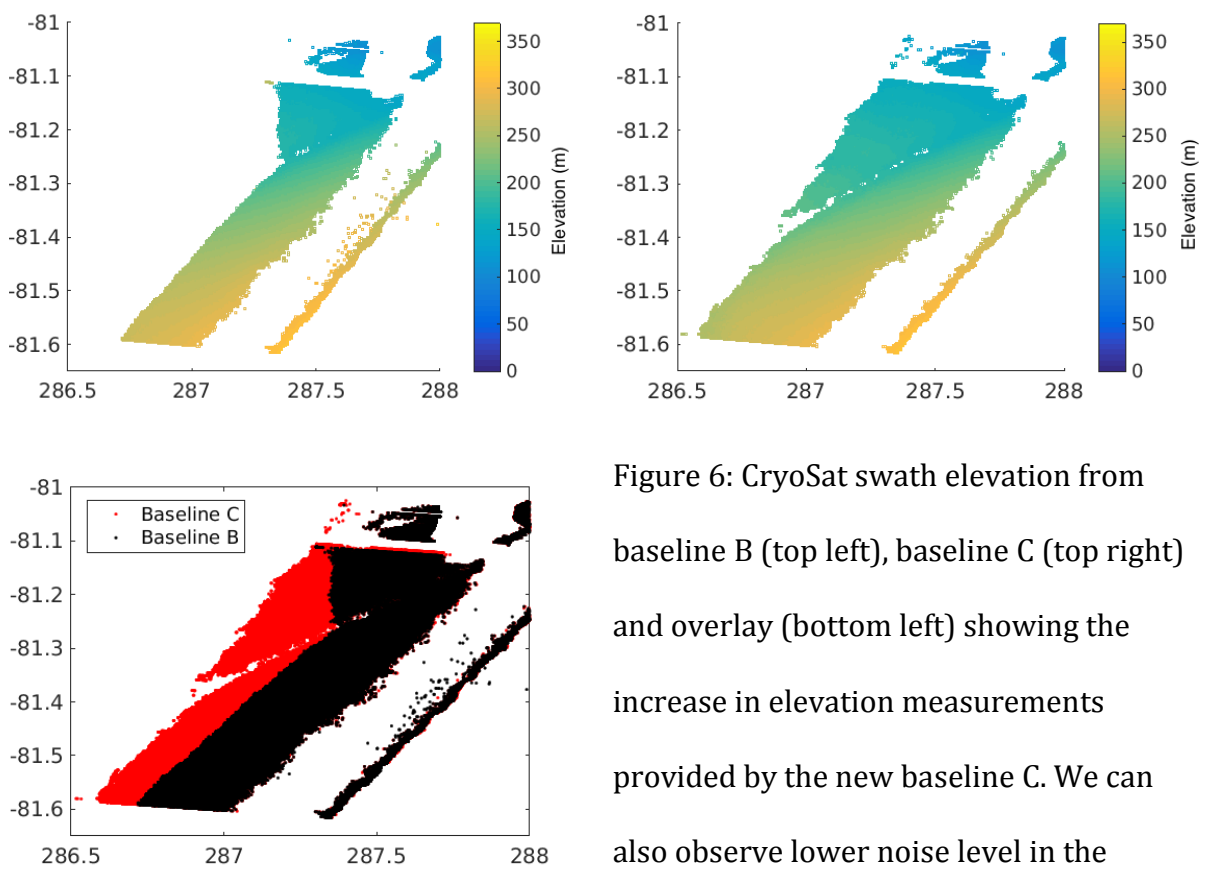


Figure 6: CryoSat swath elevation from baseline B (top left), baseline C (top right) and overlay (bottom left) showing the increase in elevation measurements provided by the new baseline C. We can also observe lower noise level in the baseline C product near the waveform's leading edge (top) as described by (Scagliola, Fornari 2015).

1
2
3
4
5
6
7
8
9
10
11
12
13
14
15
16
17
18
19
20
21
22
23
24
25
26
27
28
29
30
31
32
33
34
35
36
37
38
39
40
41
42
43
44
45
46
47
48
49
50
51
52
53
54
55
56
57
58
59
60
61
62
63
64
65

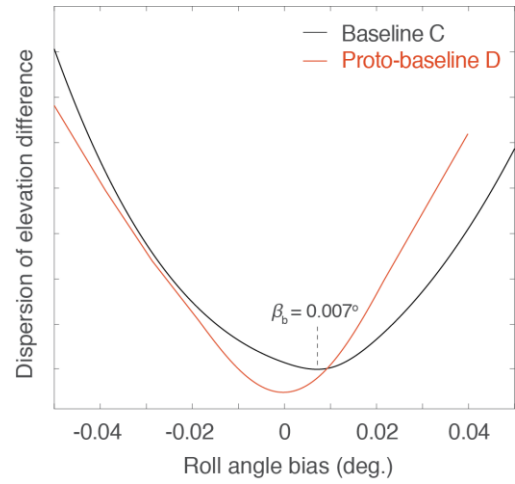
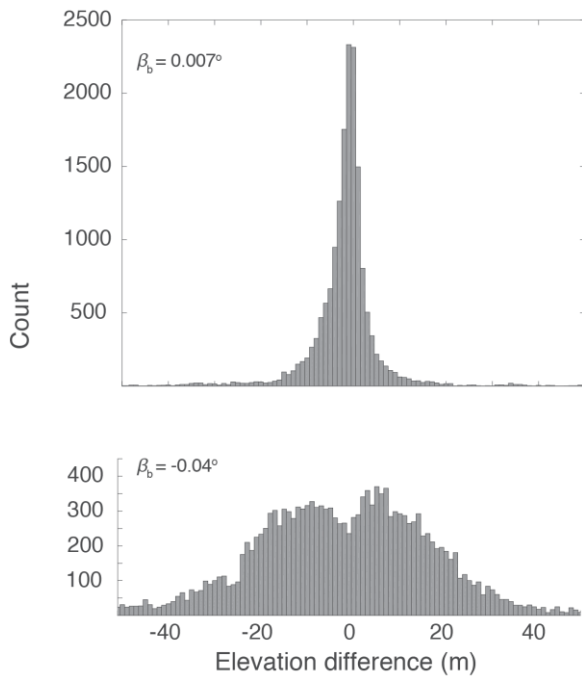


Figure 7: Distribution of 39139 L2swath elevation minus OIB elevation over the Jakobshavn area (Figure 8) with respect to experimental roll angle bias $\beta_b = 0.007^\circ$ and -0.04° (left). The roll bias that minimises the dispersion of the elevation difference is found at $\beta_b = 0.007^\circ$ (right). The same exercise using recently released corrected attitude information (Proto-baseline D data) shows that the roll angle is significantly improved (right).

1
2
3
4
5
6
7
8
9
10
11
12
13
14
15
16
17
18
19
20
21
22
23
24
25
26
27
28
29
30
31
32
33
34
35
36
37
38
39
40
41
42
43
44
45
46
47
48
49
50
51
52
53
54
55
56
57
58
59
60
61
62
63
64
65

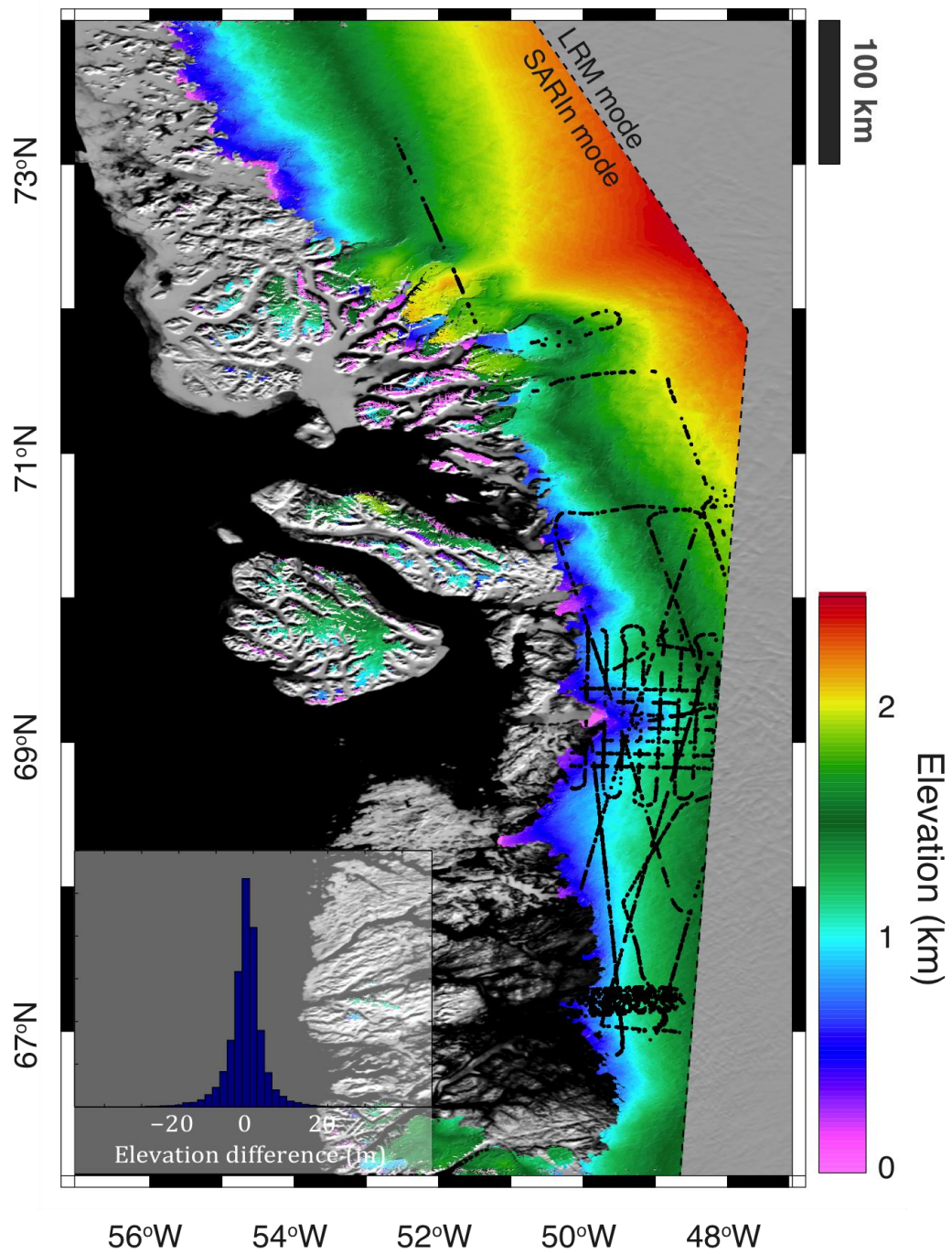


Figure 8: CryoTop L2swath continuous elevation at 500 m posting along the west coast of the GrIS overlaid over the MEaSUREs MODIS Mosaic of Greenland (Haran et al. 2013). The inland limit of the L2swath DEM corresponds to the CryoSat-2's SARIn mode mask (dashed line), elsewhere the ice mask is according to the GIMP dataset (Howat, Negrete & Smith 2014). IceBridge elevation acquired in March, April and May 2011 (black) and elevation difference with L2swath elevation for 39139 collocated measurements (inset).

1
2
3
4
5
6
7
8
9
10
11
12
13
14
15
16
17
18
19
20
21
22
23
24
25
26
27
28
29
30
31
32
33
34
35
36
37
38
39
40
41
42
43
44
45
46
47
48
49
50
51
52
53
54
55
56
57
58
59
60
61
62
63
64
65

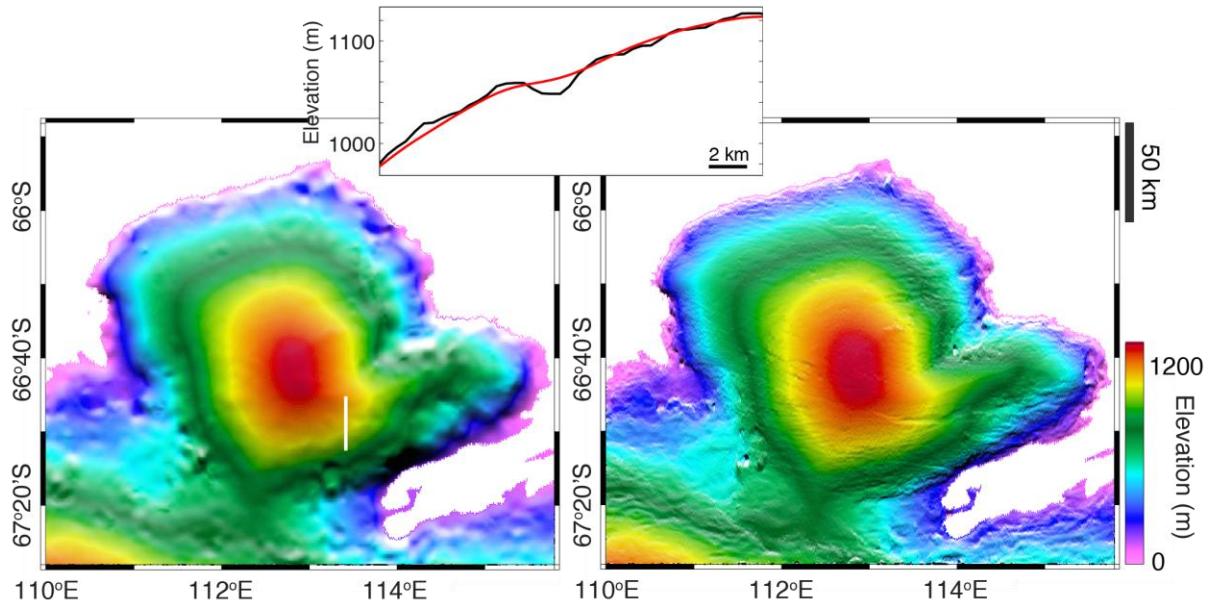


Figure 9: A continuous digital elevation model of the Law Dome, East Antarctica, (top left) from Bedmap2 posted at 1000m grid spacing (Fretwell et al. 2013), (top right) from swath mode interferometry posted at 500 m grid spacing and precise to within 2 metres. A profile (white line) shows example of small-scale features imaged by high resolution. Bedrock elevation is also shown (bottom left) (Fretwell et al. 2013).

1
2
3
4
5
6
7
8
9
10
11
12
13
14
15
16
17
18
19
20
21
22
23
24
25
26
27
28
29
30
31
32
33
34
35
36
37
38
39
40
41
42
43
44
45
46
47
48
49
50
51
52
53
54
55
56
57
58
59
60
61
62
63
64
65

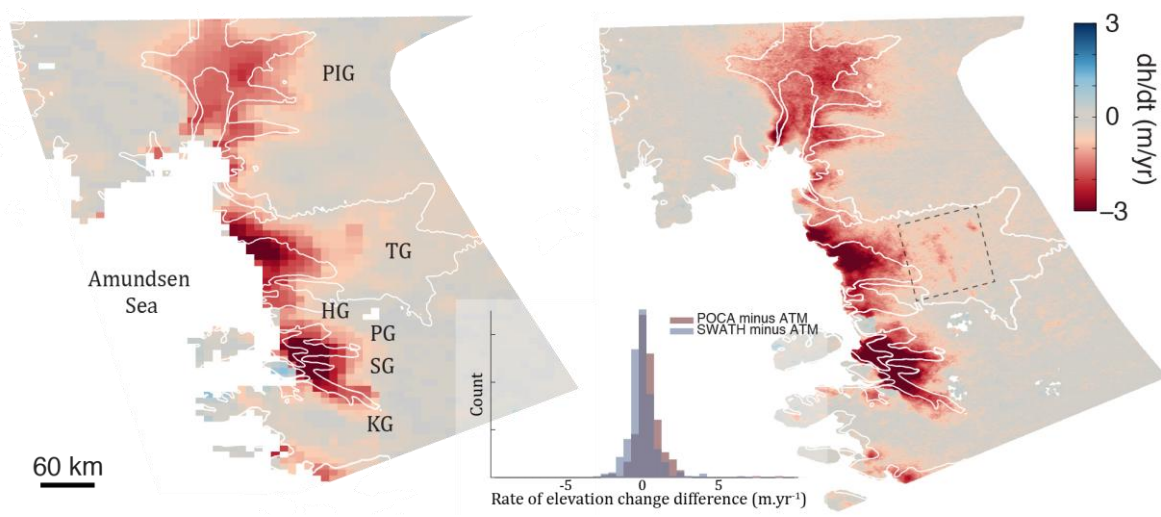


Figure 10: Surface elevation change over the Amundsen Sea Sector (left) mapped, continuously, with 10km grid spacing; (right) mapped, continuously, with 500 metre grid spacing (10 times finer than previous assessments) and an estimated precision of 0.2 m a⁻¹. Named glaciers are Pine Island (PIG), Thwaites (TG), Haynes (HG), Pope (PG), Smith (SG), Kohler (KG), the dashed area is the location of sub-glacial lakes (Figure 14). The mean difference between swath-derived rates of elevation change and airborne measurement is 0.04 ± 0.92 m a⁻¹, for comparison, the difference between POCA-derived rates of elevation change and airborne measurement is 0.40 ± 0.95 m a⁻¹ (McMillan et al. 2014b).

1
2
3
4
5
6
7
8
9
10
11
12
13
14
15
16
17
18
19
20
21
22
23
24
25
26
27
28
29
30
31
32
33
34
35
36
37
38
39
40
41
42
43
44
45
46
47
48
49
50
51
52
53
54
55
56
57
58
59
60
61
62
63
64
65

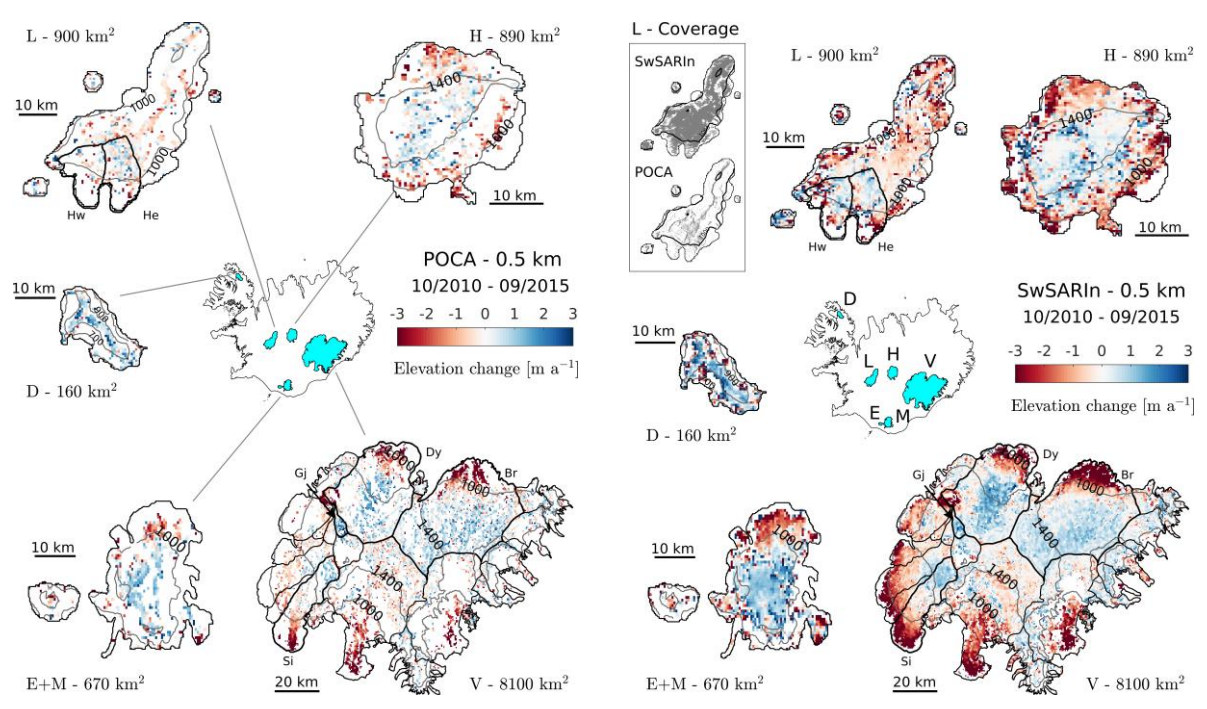


Figure 11: Rates of surface elevation for Icelandic ice caps determined from POCA (left) and L2swath (right) (Foresta et al. 2016). Relative density of elevation data determined via POCA and L2swath techniques for the Langjokull ice cap is shown in the inset (right).

1
2
3
4
5
6
7
8
9
10
11
12
13
14
15
16
17
18
19
20
21
22
23
24
25
26
27
28
29
30
31
32
33
34
35
36
37
38
39
40
41
42
43
44
45
46
47
48
49
50
51
52
53
54
55
56
57
58
59
60
61
62
63
64
65

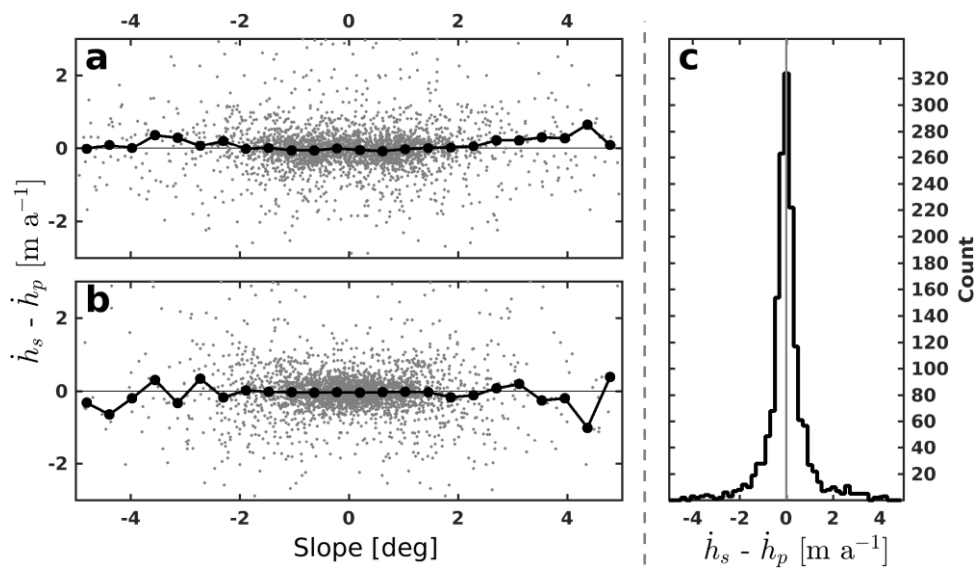


Figure 12: Difference between L2swath and POCA surface elevation change rates ($\dot{h}_s - \dot{h}_p$) over Vatnajökull with respect to (a) along-track and (b) across-track surface slope. (c) Histogram of differences between L2swath and POCA rates of surface elevation change (Foresta et al. 2016).

1
2
3
4
5
6
7
8
9
10
11
12
13
14
15
16
17
18
19
20
21
22
23
24
25
26
27
28
29
30
31
32
33
34
35
36
37
38
39
40
41
42
43
44
45
46
47
48
49
50
51
52
53
54
55
56
57
58
59
60
61
62
63
64
65

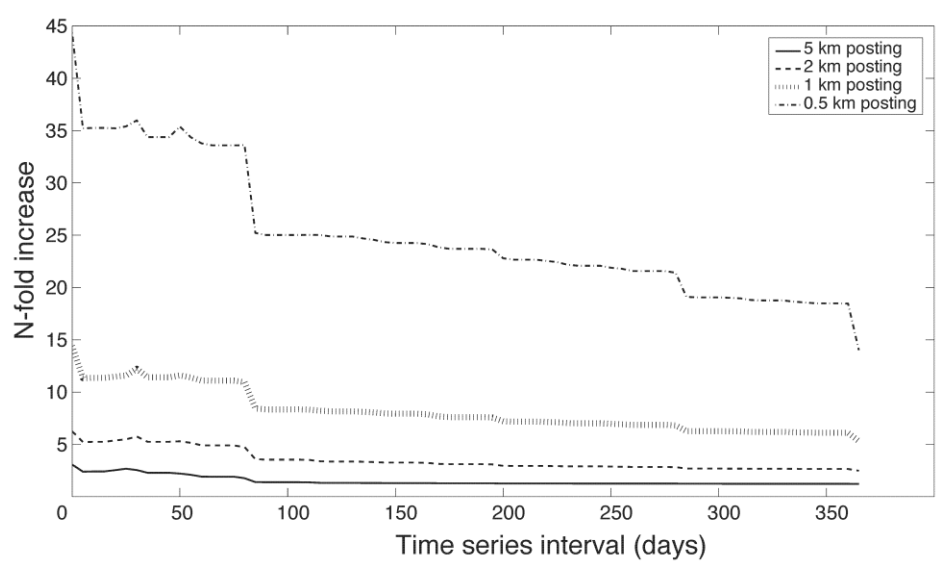


Figure 13: Increase in temporal resolution from conventional POCA to L2swath as a function of time interval and spatial posting. This has been calculated from real data over the Jakobshavn and Amundsen Sea sector areas.

1
2
3
4
5
6
7
8
9
10
11
12
13
14
15
16
17
18
19
20
21
22
23
24
25
26
27
28
29
30
31
32
33
34
35
36
37
38
39
40
41
42
43
44
45
46
47
48
49
50
51
52
53
54
55
56
57
58
59
60
61
62
63
64
65

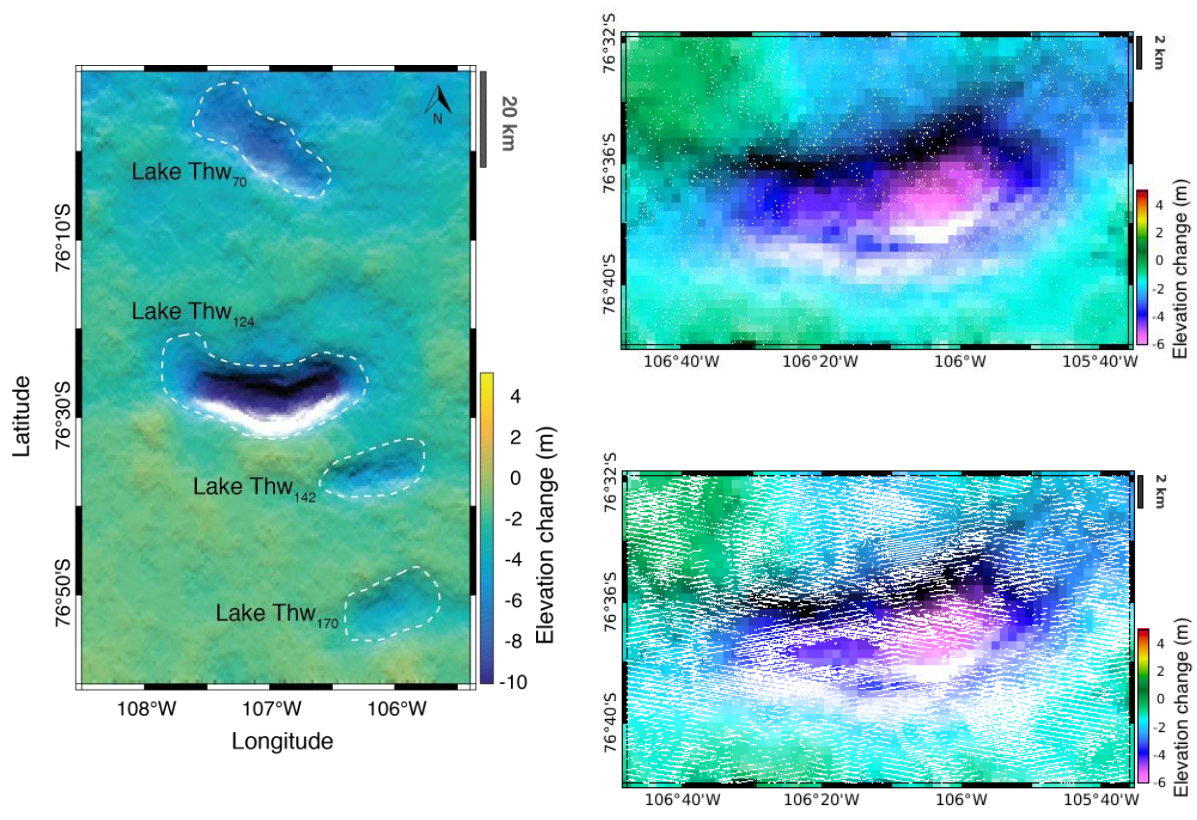


Figure 14: Surface elevation change between pre and post summer 2013 inland of the Thwaites glacier (location in Figure 10) from L2swath, showing areas of surface lowering related to the drainage of 4 subglacial lakes in mid 2013 (Smith et al. 2016). Zoom on lake Thw₁₄₂ showing the location of all measurements (white dots) acquired over a CryoSat-2 repeat cycle from POCA (top right) and from L2swath (bottom right);

background image is L2swath derived surface elevation change in both cases.

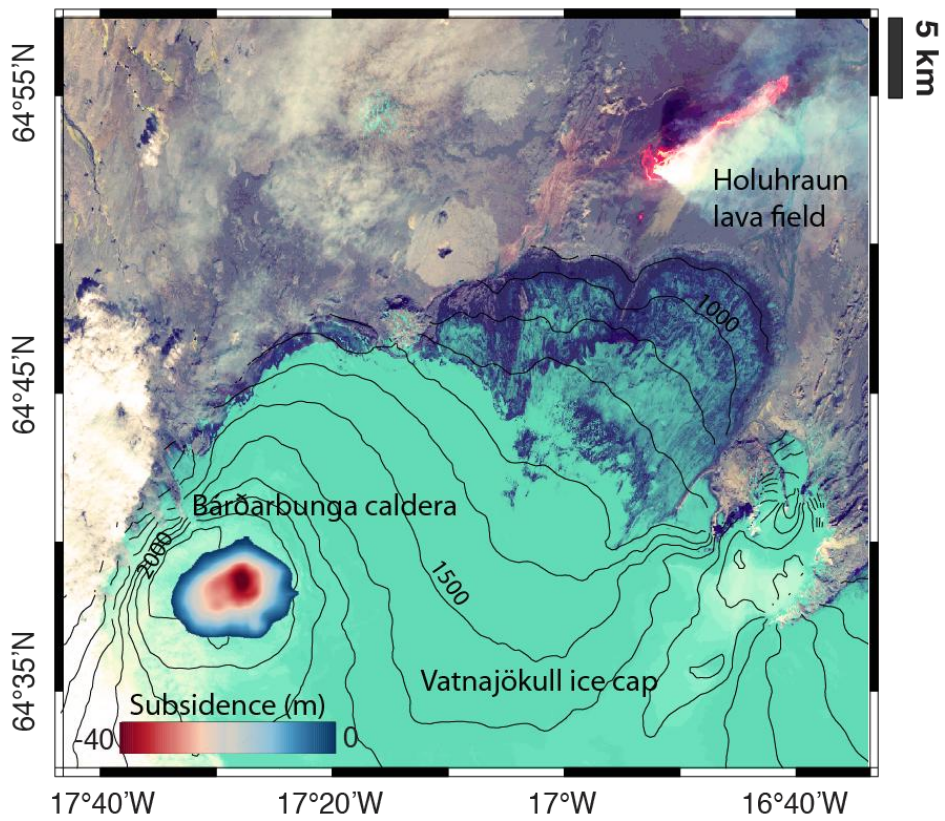


Figure 15: Rapid subsidence of the 4 km wide Bárðarbunga caldera, Vatnajökull ice cap, Iceland, after deflation of the magma chamber. Landsat-8 background image (September 6, 2014) shows contemporary Holuhraun lava flow. Elevation shown as 100 m equidistant contour lines.

1
2
3
4
5
6
7
8
9
10
11
12
13
14
15
16
17
18
19
20
21
22
23
24
25
26
27
28
29
30
31
32
33
34
35
36
37
38
39
40
41
42
43
44
45
46
47
48
49
50
51
52
53
54
55
56
57
58
59
60
61
62
63
64
65

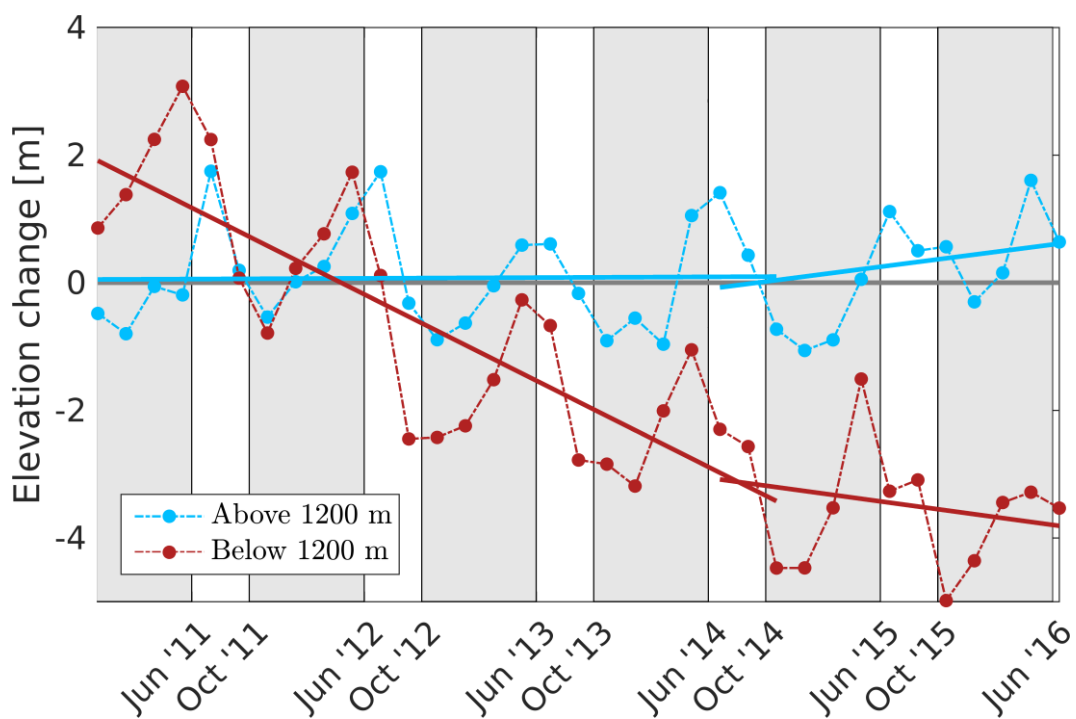


Figure 16: Vatnajökull elevation time series (60 days step) produced from L2swath elevations above and below 1200 m, used as an approximate ice cap wide ELA. The dark grey bands highlight the accumulation period between October and May; the nonshaded area corresponds to the ablation period between June and September. The two trends show mean rates of elevation change between 2010–2014 and between 2014–2016 (Foresta et al. 2016).

Table 1: Bias and dispersion of swath mode elevation and derived gridded products, POCA, with respect to Operation IceBridge Airborne Laser Scanner and comparative measurements density between POCA and swath mode

<u>Region</u>	<u>Swath elevation (m)</u>	<u>POCA elevation (m)</u>	<u>Swath/POCA Number of measures (10³)</u>	<u>Gain in spatial resolution</u>	<u>Swath DEM (m)</u>	<u>Swath dh/dt (m.a⁻¹)</u>	<u>POCA dh/dt (m.a⁻¹)</u>
Petermann	-1.3±1.2	-1.1±0.8	44.9/1.4	5 folds	NA	NA	NA
Jakobshavn	-1.2±2.0	-0.6±1.4	99.9/1.0	10 folds	-1.4±1.8	0.04±1.15	0.17±1.54
Amundsen Sea Sector	-2.0±2.0	-1.1±1.3	199.3/3.3	8 folds	-1.7±2.0	0.04±0.92	0.40±0.95

- 1 Bamber, J.L., Gomez-Dans, J.L. & Griggs, J.A. 2009, "A new 1 km digital elevation model of
2 the Antarctic derived from combined satellite radar and laser data, Part 1: Data and
3 methods", *The Cryosphere*, vol. 3, no. 1, pp. 101-111.
- 4 Bamber, J.L., Griggs, J.A., Hurkmans, R.T.W.L., Dowdeswell, J.A., Gogineni, S.P., Howat, I.,
5 Mouginot, J., Paden, J., Palmer, S., Rignot, E. & Steinhage, D. 2013, "A new bed
6 elevation dataset for Greenland", *The Cryosphere*, vol. 7, no. 2, pp. 499-510.
- 7 Berthier, E., Vincent, C., Magnússon, E., Gunnlaugsson, Á.Þ., Pitte, P., Le Meur, E.,
8 Masiokas, M., Ruiz, L., Pálsson, F., Belart, J.M.C. & Wagnon, P. 2014, "Glacier
9 topography and elevation changes derived from Pléiades sub-meter stereo images",
10 *The Cryosphere*, vol. 8, no. 6, pp. 2275-2291.
- 11 Brenner, A.C., Blnds Chadler, R.A., Thomas, R.H. & Zwally, H.J. 1983, "Slope-induced
12 errors in radar altimetry over continental ice sheets", *Journal of Geophysical
13 Research: Oceans*, vol. 88, no. C3, pp. 1617-1623.
- 14 Christie, F.D.W., Bingham, R.G., Gourmelen, N., Tett, S.F.B. & Muto, A. 2016, "Four-decade
15 record of pervasive grounding line retreat along the Bellingshausen margin of West
16 Antarctica", *Geophysical Research Letters*, vol. 43, no. 11, pp. 5741-5749.
- 17 Das, S.B., Joughin, I., Behn, M.D., Howat, I.M., King, M.A., Lizarralde, D. & Bhatia, M.P.
18 2008, "Fracture propagation to the base of the Greenland Ice Sheet during
19 supraglacial lake drainage", *Science*, vol. 320, no. 5877, pp. 778-781.
- 20 Dehecq, A., Gourmelen, N., Shepherd, A., Cullen, R. & Trouvé, E. 2013, "Evaluation of
21 CryoSat-2 for height retrieval over the Himalayan range", *CryoSat-2 third user
22 workshop*.
- 23 Dehecq, A., Millan, R., Berthier, E., Gourmelen, N., Trouvé, E. & Vionnet, V., 2016,
24 "Elevation Changes Inferred From TanDEM-X Data Over the Mont-Blanc Area:
25 Impact of the X-Band Interferometric Bias", *IEEE Journal of Selected Topics in
26 Applied Earth Observations and Remote Sensing*, vol. 9, no. 8, pp. 3870-3882.
- 27 DiMarzio, J., Brenner, A., Schutz, R., Shuman, C.A. & Zwally, H.J. 2007a, *GLAS/ICESat 1 km
28 laser altimetry digital elevation model of Greenland*, National Snow and Ice Data
29 Center, Boulder, Colorado, USA. <https://nsidc.org/data/nsidc-0305>
- 30 DiMarzio, J., Brenner, A., Schutz, R., Shuman, C.A. & Zwally, H.J. 2007b, *GLAS/ICESat 500
31 m laser altimetry digital elevation model of Antarctica*, National Snow and Ice Data
32 Center, Boulder, Colorado, USA. <https://nsidc.org/data/nsidc-0304>
- 33 Drinkwater, M.R., Ratier, G., Wingham, D. & Francis, R. 2005, "The European Space
34 Agency's Earth Explorer Mission CryoSat: Measuring Variability in the Cryosphere",
35 *Annals of Glaciology*, vol. 39, pp. 313-320.
- 36 Foresta, L., Gourmelen, N., Pálsson, F., Nienow, P., Björnsson, H. & Shepherd, A. 2016,
37 "Surface elevation change and mass balance of Icelandic ice caps derived from
38 swath mode CryoSat-2 altimetry", *Geophysical Research Letters*, vol. 43, no. 23, pp.
39 12,138-12,145.
- 40 Fretwell, P., Pritchard, H.D., Vaughan, D.G., Bamber, J.L., Barrand, N.E., Bell, R., Bianchi, C.,
41 Bingham, R.G., Blankenship, D.D., Casassa, G., Catania, G., Callens, D., Conway, H.,
42 Cook, A.J., Corr, H.F.J., Damaske, D., Damm, V., Ferraccioli, F., Forsberg, R., Fujita, S.,
43 Gim, Y., Gogineni, P., Griggs, J.A., Hindmarsh, R.C.A., Holmlund, P., Holt, J.W., Jacobel,
44 R.W., Jenkins, A., Jokat, W., Jordan, T., King, E.C., Kohler, J., Krabill, W., Riger-Kusk, M.,
45 Langley, K.A., Leitchenkov, G., Leuschen, C., Luyendyk, B.P., Matsuoka, K., Mouginot,
46 J., Nitsche, F.O., Nogi, Y., Nost, O.A., Popov, S.V., Rignot, E., Rippin, D.M., Rivera, A.,
47 Roberts, J., Ross, N., Siegert, M.J., Smith, A.M., Steinhage, D., Studinger, M., Sun, B.,
48 Tinto, B.K., Welch, B.C., Wilson, D., Young, D.A., Xiangbin, C. & Zirizzotti, A. 2013,
49
50
51
52
53
54
55
56
57
58
59
60
61
62
63
64
65

- 1 "Bedmap2: improved ice bed, surface and thickness datasets for Antarctica", *The*
2 *Cryosphere*, vol. 7, no. 1, pp. 375-393.
- 3 Fricker, H.A., Scambos, T., Bindenschadler, R. & Padman, L. 2007, "An active subglacial
4 water system in West Antarctica mapped from space", *Science*, vol. 315, no. 5818,
5 pp. 1544-1548.
- 6 Garcia-Mondejar, A., M. Fornari, M. Roca (2017) CryoSat-2: SIRAL Calibration with
7 Transponders, *Cryosat-2 Advances in Space Science*, This issue.
- 8 Gardner, A.S., Moholdt, G., Cogley, J.G., Wouters, B., Arendt, A.A., Wahr, J., Berthier, E.,
9 Hock, R., Pfeffer, W.T., Kaser, G., Ligtenberg, S.R.M., Bolch, T., Sharp, M.J., Hagen, J.O.,
10 van den Broeke, M.R. & Paul, F. 2013, "A Reconciled Estimate of Glacier
11 Contributions to Sea Level Rise: 2003 to 2009", *Science*, vol. 340, no. 6134, pp. 852-
12 857.
- 13 Gourmelen, N., Goldberg, D., Snow, K., Henley, S., Bingham, R., Kimura, S., Hogg, A.,
14 Shepherd, A., Mouginit, J., Lenearts, J., Ligtenberg, S. & van de Berg, W. 2017,
15 "Channelized melting drives thinning under a rapidly melting Antarctic ice shelf",
16 *Geophysical Research Letters*, 44, 9796–9804. 10.1002/2017GL074929.
- 17 Gray, L., Burgess, D., Copland, L., Cullen, R., Galin, N., Hawley, R. & Helm, V. 2013,
18 "Interferometric swath processing of Cryosat-2 data for glacial ice topography", *The*
19 *Cryosphere Discussions*, vol. 7, no. 3, pp. 3133-3162.
- 20 Gray, L., Burgess, D., Copland, L., Demuth, M.N., Dunse, T., Langley, K. & Schuler, T.V.
21 2015, "CryoSat-2 delivers monthly and inter-annual surface elevation change for
22 Arctic ice caps", *The Cryosphere*, vol. 9, no. 5, pp. 1895-1913.
- 23 Gray, L., Burgess, D., Copland, L., Dunse, T., Langley, K. & Moholdt, G. 2016, "Improved
24 processing and calibration of the interferometric mode of the CryoSat radar
25 altimeter allows height measurements of supraglacial lakes in west Greenland", *The*
26 *Cryosphere Discussions*, vol. 2016, pp. 1-38.
- 27 Griggs, J.A. & Bamber, J.L. 2009, "A new 1 km digital elevation model of Antarctica
28 derived from combined radar and laser data, Part 2: Validation and error
29 estimates", *The Cryosphere*, vol. 3, no. 1, pp. 113-123.
- 30 Haran, T., Bohlander, J., Scambos, T., Painter, T. & Fahnestock, M. 2013, "*MEaSUREs*
31 *MODIS Mosaic of Greenland 2005 (MOG2005) Image Map, Version 1*. Boulder,
32 Colorado USA. NSIDC: National Snow and Ice Data Center." nsidc.org/data/nsidc-0547.
- 33 Hawley, R.L., Shepherd, A., Cullen, R., Helm, V. & Wingham, D.J. 2009, "Ice-sheet
34 elevations from across-track processing of airborne interferometric radar
35 altimetry", *Geophysical Research Letters*, vol. 36, no. 22, pp. L22501.
- 36 Howat, I.M., Negrete, A. & Smith, B.E. 2014, "The Greenland Ice Mapping Project (GIMP)
37 land classification and surface elevation datasets", *The Cryosphere Discussions*, vol.
38 8, no. 1, pp. 453-478.
- 39 Howat, I.M., Porter, C., Noh, M.J., Smith, B.E. & Jeong, S. 2015, "Brief Communication:
40 Sudden drainage of a subglacial lake beneath the Greenland Ice Sheet", *The*
41 *Cryosphere*, vol. 9, no. 1, pp. 103-108.
- 42 Ignéczi, Á., Sole, A.J., Livingstone, S.J., Leeson, A., Fettweis, X., Selmes, N., Gourmelen, N. &
43 Briggs, K. 2016, "North-east sector of the Greenland Ice Sheet to undergo the
44 greatest inland expansion of supraglacial lakes during the 21st century",
45 *Geophysical Research Letters*, 43, 9729–9738, doi:[10.1002/2016GL070338](https://doi.org/10.1002/2016GL070338).
- 46 IPCC, 2013: *Climate Change 2013: The Physical Science Basis. Contribution of Working*
47 *Group I to the Fifth Assessment Report of the Intergovernmental Panel on Climate*
48 *Change* [Stocker, T.F., D. Qin, G.-K. Plattner, M. Tignor, S.K. Allen, J. Boschung, A.

- 1 Nauels, Y. Xia, V. Bex and P.M. Midgley (eds.)). Cambridge University Press,
2 Cambridge, United Kingdom and New York, NY, USA, 1535 pp,
3 doi:10.1017/CBO9781107415324.
- 4 Joughin, I., Tulaczyk, S., Fahnestock, M. & Kwok, R. 1996, "A Mini-Surge on the Ryder
5 Glacier, Greenland, Observed by Satellite Radar Interferometry", *Science*, vol. 274,
6 no. 5285, pp. 228-230.
- 7 Kaab, A., Berthier, E., Nuth, C., Gardelle, J. & Arnaud, Y. 2012, "Contrasting patterns of
8 early twenty-first-century glacier mass change in the Himalayas", *Nature*, vol. 488,
9 no. 7412, pp. 495-498.
- 10 Krabill, W.B. 2016, "*IceBridge ATM L2 Icessn Elevation, Slope, and Roughness, Version 2.*
11 ", Boulder, Colorado USA. NASA National Snow and Ice Data Center Distributed Active
12 Archive Center. <http://nsidc.org/data/ilatm2>
- 13 Krabill, W.B. 2015, *IceBridge ATM L4 Surface Elevation Rate of Change*, NASA National
14 Snow and Ice Data Center Distributed Active Archive Center., Boulder Colorado,
15 USA. <https://nsidc.org/data/IDHDT4>
- 16 Lewis, A.R., Marchant, D.R., Kowalewski, D.E., Baldwin, S.L. & Webb, L.E. 2006, "The age
17 and origin of the Labyrinth, western Dry Valleys, Antarctica: Evidence for extensive
18 middle Miocene subglacial floods and freshwater discharge to the Southern Ocean",
19 *Geology*, vol. 34, no. 7, pp. 513-516.
- 20 Liestl, O., Repp, K. & Wold, B. 1980, "Supra-glacial lakes in Spitsbergen", *Norsk*
21 *Geografisk Tidsskrift*, vol. 34, pp. 89-92.
- 22 Martin, C.F., Krabill, W.B., Manizade, S.S., Russell, R.L., Sonntag, J.G., Swift, R.N. & Yungel,
23 J.K. 2012, *Airborne topographic mapper calibration procedures and accuracy*
24 *assessment*, Greenbelt, Md.: National Aeronautics and Space Administration,
25 Goddard Space Flight Center, 2012, NASA/TM-2012-215891.
- 26 McMillan, M., Corr, H., Shepherd, A., Ridout, A., Laxon, S. & Cullen, R. 2013, "Three-
27 dimensional mapping by CryoSat-2 of subglacial lake volume changes", *Geophysical*
28 *Research Letters*, vol. 40, no. 16, pp. 4321-4327.
- 29 McMillan, M., Leeson, A., Shepherd, A., Briggs, K., Armitage, T.W.K., Hogg, A., Munneke,
30 P.K., van den Broeke, M., Brice, N., van de Berg, W.J., Ligtenberg, S., Horwath, M.,
31 Groh, A., Muir, A. & Gilbert, L. 2016, "A high resolution record of Greenland mass
32 balance", *Geophysical Research Letters*, 43, 7002–7010,
33 doi:10.1002/2016GL069666.
- 34 McMillan, M., Nienow, P., Shepherd, A., Benham, T. & Sole, A. 2007, "Seasonal evolution
35 of supra-glacial lakes on the Greenland Ice Sheet", *Earth and Planetary Science*
36 *Letters*, vol. 262, no. 3-4, pp. 484-492.
- 37 McMillan, M., Shepherd, A., Gourmelen, N., Dehecq, A., Leeson, A., Ridout, A., Flament, T.,
38 Hogg, A., Gilbert, L., Benham, T., van den Broeke, M., Dowdeswell, J.A., Fettweis, X.,
39 Noël, B. & Strozzi, T. 2014a, "Rapid dynamic activation of a marine-based Arctic ice
40 cap", *Geophysical Research Letters*, 41, 8902–8909, doi:10.1002/2014GL062255.
- 41 McMillan, M., Shepherd, A., Sundal, A., Briggs, K., Muir, A., Ridout, A., Hogg, A. &
42 Wingham, D. 2014b, "Increased ice losses from Antarctica detected by CryoSat-2",
43 *Geophysical Research Letters*, vol. 41, no. 11, pp. 3899-3905.
- 44 Phillips, T., Rajaram, H. & Steffen, K. 2010, "Cryo-hydrologic warming: A potential
45 mechanism for rapid thermal response of ice sheets", *Geophysical Research Letters*,
46 vol. 37, no. 20, L20503.
- 47 Pritchard, H.D., Arthern, R.J., Vaughan, D.G. & Edwards, L.A. 2009, "Extensive dynamic
48 thinning on the margins of the Greenland and Antarctic ice sheets", *Nature*, vol. 461,
49 no. 7266, pp. 971-975.
- 50
51
52
53
54
55
56
57
58
59
60
61
62
63
64
65

- 1 Reykjavik Institute of Earth Sciences, *Bárðarbunga* subsidence. Available:
2 <http://en.vedur.is/earthquakes-and-volcanism/articles/nr/3023>.
- 3 Scagliola, M. & Fornari, M. 2015, *Main evolutions and expected quality improvements in*
4 *BaselineC Level1b products*, no. 1.3, C2-TN-ARS-GS-5154.
- 5 Scambos, T.A., Hulbe, C., Fahnestock, M. & Bohlander, J. 2000, "The link between climate
6 warming and break up of ice shelves in the Antarctic Peninsula", *Journal of*
7 *Glaciology*, vol. 46, no. 154, pp. 516-530.
- 8 Schenk, T., Csatho, B. & Lee, D.C. 1999, "Quality control issues of airborne laser ranging
9 data and accuracy study in an urban area ", *IAPRS*, La Jolla, California, Vol. 32, Part
10 3W14, 8 pages.
- 11 Shepherd, A., Wingham, D., Payne, T. & Skvarca, P. 2003, "Larsen ice shelf has
12 progressively thinned", *Science*, vol. 302, no. 5646, pp. 856-859.
- 13 Shepherd, A., Wingham, D.J., Mansley, J.A.D. & Corr, H.F.J. 2001, "Inland thinning of Pine
14 Island Glacier, West Antarctica", *Science*, vol. 291, no. 5505, pp. 862-864.
- 15 Shepherd, A., Ivins, E.R., A, G., Barletta, V.R., Bentley, M.J., Bettadpur, S., Briggs, K.H.,
16 Bromwich, D.H., Forsberg, R., Galin, N., Horwath, M., Jacobs, S., Joughin, I., King, M.A.,
17 Lenaerts, J.T.M., Li, J., Ligtenberg, S.R.M., Luckman, A., Luthcke, S.B., McMillan, M.,
18 Meister, R., Milne, G., Mouginot, J., Muir, A., Nicolas, J.P., Paden, J., Payne, A.J.,
19 Pritchard, H., Rignot, E., Rott, H., Sørensen, L.S., Scambos, T.A., Scheuchl, B., Schrama,
20 E.J.O., Smith, B., Sundal, A.V., van Angelen, J.H., van de Berg, W.J., van den Broeke,
21 M.R., Vaughan, D.G., Velicogna, I., Wahr, J., Whitehouse, P.L., Wingham, D.J., Yi, D.,
22 Young, D. & Zwally, H.J. 2012, "A Reconciled Estimate of Ice-Sheet Mass Balance",
23 *Science*, vol. 338, no. 6111, pp. 1183-1189.
- 24 Siegert, M.J., Carter, S., Tabacco, I., Popov, S. & Blankenship, D.D. 2005, "A revised
25 inventory of Antarctic subglacial lakes", *Antarctic Science*, vol. 17, no. 03, pp. 453-
26 460.
- 27 Sigmundsson, F., Hooper, A., Hreinsdottir, S., Vogfjord, K.S., Ofeigsson, B.G., Heimisson,
28 E.R., Dumont, S., Parks, M., Spaans, K., Gudmundsson, G.B., Drouin, V., Arnadottir, T.,
29 Jonsdottir, K., Gudmundsson, M.T., Hognadottir, T., Fridriksdottir, H.M., Hensch, M.,
30 Einarsson, P., Magnusson, E., Samsonov, S., Brandsdottir, B., White, R.S.,
31 Agustsdottir, T., Greenfield, T., Green, R.G., Hjartardottir, A.R., Pedersen, R., Bennett,
32 R.A., Geirsson, H., La Femina, P.C., Bjornsson, H., Palsson, F., Sturkell, E., Bean, C.J.,
33 Mollhoff, M., Braiden, A.K. & Eibl, E.P.S. 2015, "Segmented lateral dyke growth in a
34 rifting event at Bárðarbunga volcanic system, Iceland", *Nature*, vol. 517, no. 7533,
35 pp. 191-195.
- 36 Smith, B. E., Fricker, H.A., Joughin, I.R. & Tulaczyk, S. 2009, "An inventory of active
37 subglacial lakes in Antarctica detected by ICESat (2003–2008)", *Journal of*
38 *Glaciology*, vol. 55, no. 192, pp. 573-595.
- 39 Smith, B.E., Gourmelen, N., Huth, A. & Joughin, I. 2016, "Connected subglacial lake
40 drainage beneath Thwaites Glacier, West Antarctica", *The Cryosphere Discussions*,
41 vol. 2016, pp. 1-19.
- 42 Stearns, L.A., Smith, B.E. & Hamilton, G.S. 2008, "Increased flow speed on a large East
43 Antarctic outlet glacier caused by subglacial floods", *Nature Geosci*, vol. 1, no. 12, pp.
44 827-831.
- 45 Wilson, W. S., Abdalati, W., Alsdorf, D., Benveniste, J., Bonekamp, H., Cogley, J. G.,
46 Drinkwater, M. R., Fu, L.-L., Gross, R., Haines, B. J., Harrison, D. E., Johnson, G. C.,
47 Johnson, M., LaBrecque, J. L., Lindstrom, E. J., Merrifield, M. A., Miller, L., Pavlis, E. C.,
48 Piotrowicz, S., Roemmich, D., Stammer, D., Thomas, R. H., Thouvenot, E. and
49 Woodworth, P. L. 2010, "Observing Systems Needed to Address Sea-Level Rise and
50
51
52
53
54
55
56
57
58
59
60
61
62
63
64
65

Variability”, in Understanding Sea-Level Rise and Variability (eds J. A. Church, P. L. Woodworth, T. Aarup and W. S. Wilson), Wiley-Blackwell, Oxford, UK. doi: 10.1002/9781444323276.ch12

Wingham, D.J., Francis, C.R., Baker, S., Bouzinac, C., Brockley, D., Cullen, R., de Chateau-Thierry, P., Laxon, S.W., Mallow, U., Mavrocordatos, C., Phalippou, L., Ratier, G., Rey, L., Rostan, F., Viau, P. & Wallis, D.W. 2006, “CryoSat: A mission to determine the fluctuations in Earth's land and marine ice fields”, *Advances in Space Research*, 37, 841–871.

Wingham, D.J., Ridout, A., Scharroo, R., Arthern, R. & Shum, C.K. 1998, "Antarctic elevation change from 1992 to 1996", *Science*, vol. 282, no. 5388, pp. 456-458.

Wingham, D.J., Shepherd, A., Muir, A. & Marshall, G.J. 2006a, "Mass balance of the Antarctic ice sheet", *Philosophical Transactions of the Royal Society A-Mathematical Physical and Engineering Sciences*, vol. 364, no. 1844, pp. 1627-1635.

Wingham, D.J., Siegert, M.J., Shepherd, A. & Muir, A.S. 2006b, "Rapid discharge connects Antarctic subglacial lakes", *Nature*, vol. 440, no. 7087, pp. 1033-1036.

Wright, A. & Siegert, M. 2012, "A fourth inventory of Antarctic subglacial lakes", *Antarctic Science*, vol. 24, no. 06, pp. 659-664.

Zwally, H.J., Brenner, A.C., Major, J.A., Bindschadler, R.A. & Marsh, J.G. 1989, "Growth of Greenland Ice-Sheet - Measurement", *Science*, vol. 246, no. 4937, pp. 1587-1589.

Zwally, H.J., Giovinetto, M.B., Li, J., Cornejo, H.G., Beckley, M.A., Brenner, A.C., Saba, J.L. & Yi, D.H. 2005, "Mass changes of the Greenland and Antarctic ice sheets and shelves and contributions to sea-level rise: 1992-2002", *Journal of Glaciology*, vol. 51, no. 175, pp. 509-527.

Editor:

Editor's comments:

I have again reviewed the references and find the following need additional information. Once these references are complete the paper will be accepted.

*Gourmelen, N., Goldberg, D., Snow, K., Henley, S., Bingham, R., Kimura, S., Hogg, A., Shepherd, A., Mougnot, J., Lenearts, J., Ligtenberg, S. & van de Berg, W. 2017, "Channelized melting drives thinning under a rapidly melting Antarctic ice shelf", *Geophysical Research Letters*, 10.1002/2017GL074929.*

Volume number and inclusive page numbers are missing.

*Ignéczi, Á., Sole, A.J., Livingstone, S.J., Leeson, A., Fettweis, X., Selmes, N., Gourmelen, N. & Briggs, K. 2016, "North-east sector of the Greenland Ice Sheet to undergo the greatest inland expansion of supraglacial lakes during the 21st century", *Geophysical Research Letters*, , pp. n/a-n/a.*

Volume number and inclusive page numbers are missing.

*IPCC 2013, *Climate Change 2013 - The Physical Science Basis. Contribution of Working Group I to the Fifth Assessment Report of the IPCC*, Cambridge University Press.*

The publisher's city is missing.

*Martin, C.F., Krabill, W.B., Manizade, S.S., Russell, R.L., Sonntag, J.G., Swift, R.N. & Yungel, J.K. 2012, *Airborne topographic mapper calibration procedures and accuracy assessment, Greenbelt, Md.: National Aeronautics and Space Administration, Goddard Space Flight Center, 2012**

The NASA technical report number should be cited. It is NASA/TM-2012-215891

*McMillan, M., Leeson, A., Shepherd, A., Briggs, K., Armitage, T.W.K., Hogg, A., Munneke, P.K., van den Broeke, M., Brice, N., van de Berg, W.J., Ligtenberg, S., Horwath, M., Groh, A., Muir, A. & Gilbert, L. 2016, "A high resolution record of Greenland mass balance", *Geophysical Research Letters*.*

Volume number and inclusive page numbers are missing.

*McMillan, M., Shepherd, A., Gourmelen, N., Dehecq, A., Leeson, A., Ridout, A., Flament, T., Hogg, A., Gilbert, L., Benham, T., van den Broeke, M., Dowdeswell, J.A., Fettweis, X., Noël, B. & Strozzi, T. 2014a, "Rapid dynamic activation of a marine-based Arctic ice cap", *Geophysical Research Letters*, 2014GL062255.*

Volume number and inclusive page numbers are missing.

*Phillips, T., Rajaram, H. & Steffen, K. 2010, "Cryo-hydrologic warming: A potential mechanism for rapid thermal response of ice sheets", *Geophysical Research Letters*, vol. 37, no. 20.*

The paper number is missing. It is L20503.

*Scagliola, M. & Fornari, M. 2015, *Main evolutions and expected quality improvements in BaselineC Level1b products.**

Reference is incomplete.

Schenk, T., Csatho, B. & Lee, D.C. 1999, "Quality control issues of airborne laser ranging data and accuracy study in an urban area ", pp. 101.

Reference is incomplete.

*Wilson, W.S., Abdelati, W., Alsdorf, D., Benveniste, J., Bonekamp, H., Cogley, J.G., Drinkwater, M.R., Fu, L.L., Gross, R., Haines, B.J., Harrison, D.E., Johnson, G.C., Johnson, M., LaBrecue, J., Lindstrom, E.J., Merrifield, M.A., Miller, L., Pavlis, E.C., Petrovicz, S., Roemmich, D., Stammer, D., Thomas, R.H., Thouvenot, E. & Woodworth, P.L. 2010, "Observing Systems Needed to Address Sea-Level Rise and Variability" in *Understanding Sea-Level Rise and Variability*, ed. Church, J.A., P.L. Woodworth, T. Aarup, and W.S. Wilson, Wiley-Blackwell, , pp. 376-399.*

The publisher's city is missing.

I also noted that many of your references are items from the NASA National Snow and Ice Data Center Distributed Active Archive Center in Boulder. It would be nice (but not required) to give the web site.

Response:

All references have been corrected and link to NSIDC added.